



1 Factors controlling spatiotemporal variability of soil carbon accumulation and stock estimates in a tidal

2 salt marsh

3 Author Information:

4 <sup>1,5</sup> Sean Fettrow ORCID: 0000-0003-1191-4484

5 <sup>2</sup> Andrew Wozniak ORCID: 0000-0002-7079-3144

6 <sup>3,4</sup> Holly A. Michael ORCID: 0000-0003-1107-7698

7 <sup>1,3</sup> Angelia L. Seyfferth ORCID: 0000-0003-3589-6815

8

9 <sup>1</sup>Department of Plant and Soil Sciences, University of Delaware, Newark DE, USA

10 <sup>2</sup>School of Marine Science and Policy, University of Delaware, Lewes DE, USA

11 <sup>3</sup>Department of Earth Sciences, University of Delaware, Newark DE, USA

12 <sup>4</sup>Department of Civil and Environmental Engineering, University of Delaware, Newark, DE, USA

13 <sup>5</sup>Oak Ridge National Laboratory, Environmental Sciences Division

14

15 \* Corresponding Author: Angelia Seyfferth, [angelias@udel.edu](mailto:angelias@udel.edu)

16

17



18 **Abstract**

19 Tidal salt marshes are important contributors to soil carbon (C) stocks despite their relatively small land  
20 surface area. Although it is well understood that salt marshes have soil C burial rates orders of magnitude  
21 greater than those of terrestrial ecosystems, there is a wide range in storage rates among spatially  
22 distributed marshes. In addition, wide ranges in C storage rates also exist within a single marsh  
23 ecosystem. Tidal marshes often contain multiple species of cordgrass due to variations in hydrology and  
24 soil biogeochemistry caused by microtopography and distance from tidal creeks, creating distinct subsites.  
25 Our overarching objective was to observe how soil C concentration changes across four plant  
26 phenophases and across three subsites categorized by unique vegetation, hydrology, and biogeochemistry,  
27 while also investigating dominant biogeochemical controls on soil C concentration. We hypothesized that  
28 subsite biogeochemistry drives spatial heterogeneity in soil C concentration, and this causes variability in  
29 soil C concentration at the marsh scale. In addition, we hypothesized that soil C concentration and  
30 porewater biogeochemistry vary temporally across the four plant phenophases (i.e., senescence,  
31 dormancy, green-up, maturity), causing further variation in marsh soil C that could lead to uncertainty in  
32 soil C estimates. To test these hypotheses, we quantified soil C concentrations in 12 cm sections of soil  
33 cores (0-48 cm depth) across time (i.e., phenophase) and space (i.e., subsite), alongside several porewater  
34 biogeochemical variables including dissolved organic carbon (DOC), EEMs/ UV-VIS, redox potential,  
35 pH, salinity, reduced iron ( $\text{Fe}^{2+}$ ), reduced sulfur ( $\text{S}^{2-}$ ), and total porewater element (Fe, Ca) concentrations  
36 in three distinct subsites. Soil C concentration varied significantly ( $p < 0.05$ ) among the three subsites and  
37 was significantly greater during plant dormancy. Soil S, porewater sulfide, redox potential, and depth  
38 predicted 44% of the variability in soil C concentration. Our results show that soil C varied spatially  
39 across a marsh ecosystem up to 63% and across plant phenophase by 26%, causing variability in soil C  
40 storage rates and stocks depending on where and when samples are taken. This shows that hydrology,  
41 biogeochemistry, and ecological function are major controls on saltmarsh C content. It is, therefore,  
42 critical to consider spatial and temporal heterogeneity in soil C concentration when conducting blue C  
43 assessments to account for soil carbon variability and uncertainty in C stock estimates.



44

## 45 **1 Introduction**

46 Coastal blue carbon (C) cycled in tidal salt marshes is critically important for global soil C  
47 sequestration despite the small relative land area (Mcowen et al. 2017). High primary productivity  
48 coupled with high sedimentation rates and slowed organic C decomposition due to flooded anoxic soils  
49 allow salt marshes to rapidly accrete and preserve soil C (Arias-Ortiz et al. 2018). Soils in such  
50 ecosystems retain approximately 15% of their yearly primary productivity in soils compared to just 1%  
51 for tropical rainforests (Duarte 2017). Restoring, protecting, and artificially creating salt marshes can  
52 facilitate removal of CO<sub>2</sub> from the atmosphere and storage in soils on timescales conducive to climate  
53 change mitigation goals. These ecosystems should therefore be included in climate mitigation policy  
54 (Ewers Lewis et al. 2019; Serrano et al. 2019). However, a wide range of global salt marsh soil C  
55 sequestration rates of ~ 1 to >1100 g C m<sup>-2</sup> year<sup>-1</sup> has been reported (Wang et al. 2021). The inclusion of  
56 salt marshes in improved climate mitigation policy is, in part, contingent upon improving our  
57 understanding of the environmental variables causing wide ranges in marsh soil C concentration and thus  
58 soil sequestration rates (Saintilan et al. 2013; Macreadie et al. 2019). Understanding key controls on salt  
59 marsh soil C variability will also decrease uncertainty in Earth System Models and inform new policy  
60 aimed at protecting these valuable ecosystems.

61 Soil C concentrations in salt marsh ecosystems vary spatially across the globe. Part of this  
62 variation is explained by regional environmental controls such as average annual air temperature (Chmura  
63 et al. 2003), geomorphic setting (van Ardenne et al. 2018), salinity gradients, inundation frequency (van  
64 de Broek et al. 2016; Baustian et al. 2017; Luo et al. 2019), rainfall patterns (Sanders et al. 2016;  
65 Negandhi et al. 2019), soil pH, soil moisture, and the dominant plant species and soils (Bai et al. 2016;  
66 Ford et al. 2019). Soil C accumulation rates also vary based on the age of the marsh and tend to be highest  
67 in newly expanding marsh edges (Miller et al. 2022). Other logistical factors contributing to variability  
68 and heterogeneity in salt marsh blue C estimates include the type of corer used (Smeaton et al. 2020) and



69 the depth of soil that is integrated into storage rates (Bai et al. 2016; Van De Broek et al. 2016; Mueller et  
70 al. 2019). While understanding global and regional controls on soil C is important for reducing  
71 uncertainty in C estimates, understanding site-level factors is also critical because ecosystem-level  
72 variability can be just as high as regional- to global-level variability (Ewers Lewis et al. 2018).  
73 Belowground biogeochemical heterogeneity is often noticeable in the aboveground vegetation due to  
74 striking zonation of marsh grass species across the marsh platform. This is often attributable to small  
75 spatial-scale changes in hydrologic patterns (Guimond et al. 2020b, a) based on proximity to the tidal  
76 channel that drives unique subsite biogeochemistry (Seyfferth et al. 2020) which subsequently determines  
77 the type of vegetation that can survive within a given tidal zone (Davy et al. 2011). While tidal zonation  
78 alters vegetation and belowground biogeochemistry, it remains unclear if soil C concentrations are  
79 directly or indirectly altered by these dynamics.

80 Primary production rates may partially control soil C concentration and may vary among  
81 vegetative zones. For example, the short form of *Spartina alterniflora* has a lower primary production rate  
82 than the tall form (Roman and Daiber 1984) and *Phragmites australis* has above and below ground  
83 production rates two times that of the shorter *Spartina patens* (Windham 2001). Belowground  
84 productivity includes root exudates (Luo et al. 2018) in the form of dissolved organic carbon (DOC),  
85 which could influence soil C concentration because belowground productivity often exceeds above  
86 ground productivity in these ecosystems (Frasco and Good 1982). Even though DOC exudates are  
87 considered to be labile (Yousefi Lalimi et al. 2018), they may contribute to soil C accumulation over time  
88 due to microbial transformation (Valle et al. 2018) and association with soil minerals such as Fe oxides  
89 (Chen et al. 2014; Chen and Sparks 2015; Sowers et al. 2018a, b, 2019). The characterization of DOC  
90 quantified by optical properties of chromophoric dissolved organic carbon (CDOM) can also affect  
91 degradability (Clark et al. 2014) and may differ across the marsh platform.

92 Subsites can have unique biogeochemical signatures based on soil redox conditions and  
93 inundation extent and frequency. For example, high marsh areas and areas near tidal channels have soils  
94 which are at least periodically oxic to sub-oxic and are dominated by iron (III) reduction, whereas low



95 marsh areas have continuously inundated soils and are dominated by sulfate ( $\text{SO}_4^{2-}$ ) reduction (Seyfferth  
96 et al. 2020). While these biogeochemical characteristics can directly influence vegetation (Moffett and  
97 Gorelick 2016) and thus indirectly influence soil C concentrations, they may also directly affect soil C  
98 through the interactions of soil C with soil minerals. Fe oxides have an intimate role in the C cycle and C  
99 stabilization in soils experiencing dynamic redox fluctuation (Sodano et al. 2017), as previous work has  
100 shown that 99% of the dissolved Fe in the ocean is complexed with organic ligands (Whitby et al. 2020)  
101 and ~21% of all organic C in marine sediments is bound to reactive Fe species (Lalonde et al. 2012). Fe  
102 oxides may play an important role in C stabilization in soils experiencing dynamic redox fluctuation. Fe  
103 oxides can protect DOC against microbial degradation through physiochemical protection (Blair and Aller  
104 2012; Chen and Sparks 2015; Sodano et al. 2017; Sowers et al. 2018a; Dorau et al. 2019; Wordofa et al.  
105 2019), but these organo-mineral assemblages can be dissociated under reducing conditions (Riedel et al.  
106 2013; Wordofa et al. 2019; Lacroix et al. 2022; Fettrow et al. 2023a). Therefore, examining the spatial  
107 variability in soil biogeochemistry and relating those variables to soil C concentration may elucidate  
108 important mechanisms that cause the wide range in salt marsh soil C concentrations.

109         While it is critical to assess spatial heterogeneity in soil C concentration, it is also important to  
110 assess temporal variability. The temporal assessment of soil C in salt marshes often considers long-term  
111 trends of historic C burial rates (Cusack et al. 2018; McTigue et al. 2019; Breithaupt et al. 2020; Cuellar-  
112 Martinez et al. 2020), but variability of salt marsh soil C concentrations may also occur on shorter time  
113 scales such as across a single year. Several studies suggest salt marsh soil C does not significantly change  
114 across seasons throughout the year (Yu et al. 2014; Zhao et al. 2016), even though major changes in soil  
115 biogeochemical variables occur on this timescale (Koretsky et al. 2005; Negrin et al. 2011; Seyfferth et al.  
116 2020; Trifunovic et al. 2020; Zhu et al. 2021). While soil C concentration may be stable across seasons, it  
117 is unclear if soil C concentration changes based on site-specific plant phenology. The phenophase of a  
118 marsh is associated with the greenness index of vegetation (Trifunovic et al. 2020) and is strongly  
119 associated with C dynamics in wetland systems (Desai 2010; Kang et al. 2016). Soil C concentration



120 should be measured across plant phenophase to determine if temporal changes in phenology alter soil C  
121 concentration and cause another source of variability in ecosystem-scale C estimates.

122 To address these knowledge gaps, we conducted a year-long study of a temperate tidal salt marsh  
123 to assess how soil C concentration and porewater biogeochemistry change in space (subsite) and time  
124 (phenophase). Our overarching research objectives were to understand how soil C concentration and soil  
125 biogeochemistry change across spatial and temporal scales, and to investigate key biogeochemical  
126 mechanisms influencing soil C concentration at the ecosystem level. We hypothesized that subsites would  
127 contain significantly different concentrations of soil C due to differences in soil biogeochemistry across  
128 the marsh platform. We further hypothesized that soil C concentration and associated biogeochemistry  
129 would significantly differ across plant phenophase. Our results improve understanding of mechanistic  
130 controls on salt marsh soil C with implications for characterizing and reducing uncertainty in C  
131 sequestration estimates, while also adding to the body of literature that shows tidal salt marshes are  
132 critical reservoirs of sequestered C.

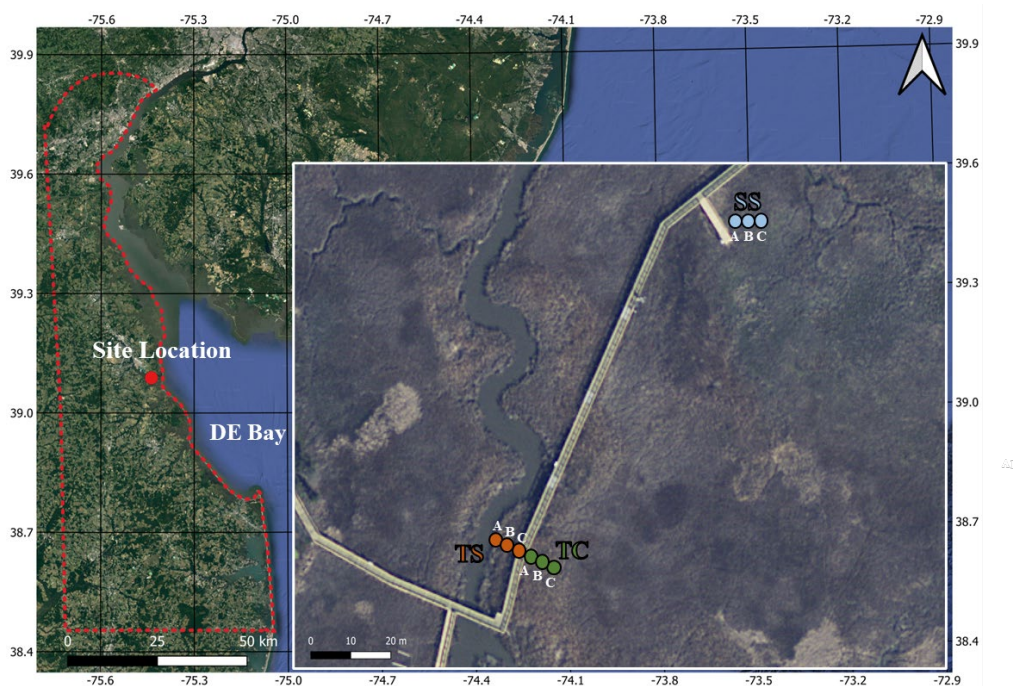
## 133 **2.0 Methods and Materials**

### 134 **2.1 Field Site**

135 This study was conducted at the St. Jones National Estuarine Research Reserve located in Dover,  
136 Delaware (Figure 1). The ecosystem is classified as a temperate mesohaline tidal salt marsh with a tidal  
137 creek salinity ranging from 5 to 18 ppt (Capooci et al. 2019). Three separate subsites were previously  
138 identified at this site, each with a different vegetation type and hydrology (Guimond et al. 2020a; Seyfferth  
139 et al. 2020). The subsite nearest the channel is primarily colonized by the tall form of *Spartina alterniflora*  
140 and has semidiurnal tidal oscillation. This subsite is hereafter referred to as Tall Spartina (TS). Farther from  
141 the tidal channel, the elevation is slightly higher due to a natural levee and flooding of the upper 25 cm of  
142 soil occurs only during spring tides; this location has the larger cordgrass *S. cynosuroides* and is hereafter  
143 referred to as Tall Cordgrass (TC). The third subsite is farthest from the tidal channel, lowest in elevation,  
144 and is primarily colonized by the short form of *S. alterniflora* due to near continuous inundation; this subsite  
145 is hereafter referred to as Short Spartina (SS). These subsites have distinct hydro-biogeochemistry and



146 vegetation that varies across small spatial scales and thus provides an ideal setting to understand site-level  
147 variability in soil C concentration, porewater biogeochemistry and their relationships.



148  
149 **Figure 1.** Map of the field site located at the St Jones Reserve near Dover, DE. Three unique subsites (TS,  
150 TC and SS) have been characterized based on previous studies at this field site showing subsite specific  
151 hydrology, vegetation, and biogeochemistry based on distance from the tidal creek (Guimond et al. 2020a;  
152 Seyfferth et al. 2020). The coring locations were sampled in triplicate (Core A, B and C), with core A  
153 starting closest to the creek and each subsequent core in each subsite being ~30cm from one another. The  
154 base layer for the map was obtained from public base layers in QGIS (© Google Maps).

155  
156  
157

## 2.2 Soil Sampling and Analysis

158 Soil cores were obtained from each of the three subsites (TS, TC, SS) in triplicate during each  
159 sampling event. Replicates were taken approximately 30cm from one another and are labeled cores A, B,  
160 and C based on distance to the tidal channel with A being closest to the channel and C the farthest (Figure  
161 1). Sampling events occurred at four separate times of the year to coincide with each of the phenophases  
162 (i.e., senescence on 10/3/2019, dormancy on 12/3/2019, green-up on 4/29/2020, maturity on 8/13/2020),  
163 which were previously determined using the Greenness Index (Trifunovic et al. 2020). Soil cores (6 cm x



164 48 cm) were extracted using a gouge auger that has been shown to be an effective coring technique for  
165 reducing compaction in soft marsh soils (Smeaton et al. 2020). Soil cores were quickly sectioned in the  
166 field into 12 cm increments (0-12cm, 12-24cm, 24-36cm and 36-48cm relative to the soil surface) and  
167 preserved under anoxic conditions following previous methods (Seyfferth et al. 2020). For reference, the  
168 rooting zone of *Spartina* grasses is between 8-20cm (Muench and Elsey-Quirk 2019), so the upper two  
169 sections likely include C from fresh root exudates. The 12cm increments were chosen because many soil  
170 C stock papers use increments between 10-15 cm and there tends to be little variation across the ~10 cm  
171 increment in a variety of wetland soils (Baustian et al. 2017). Briefly, the soil sections were placed into  
172 250 ml HDPE bottles which were left uncapped in gas-impermeable bags that contained oxygen scrubbers  
173 (AneroPack-Anero, Mitsubishi), and the bags were vacuum-sealed in the field. The soil samples were  
174 placed on ice during transport back to the lab. Once back in the lab, the soil sections in the gas-  
175 impermeable bags were immediately placed inside an anoxic glove bag containing ~5% hydrogen and  
176 ~95% nitrogen. A subsample of soil was dried, ground, sieved (2mm), and powdered for analysis of total  
177 C and S (Vario EL Cube, Elementar). Soil C and S are reported as % C (= 100% \* g C/g soil dry wt.) and  
178 % S (= 100% \* g S/g soil dry wt.). The remaining field-moist soil was left inside the HDPE vial, capped  
179 inside the glove bag, and centrifuged for extraction of porewater using methods in the following section.

### 180 **2.3 Porewater Extraction and Analysis**

181 Porewater was extracted from each 12-cm soil section by centrifugation for 2 minutes under an  
182 anoxic atmosphere at 2,500 rpm. A portion of the porewater was filtered with 0.45 $\mu$ m PTFE syringe  
183 filters while the rest was vacuum filtered using glass fiber filters (0.7 $\mu$ m). The 0.45 $\mu$ m PTFE filtered  
184 porewater was immediately analyzed for Fe<sup>2+</sup> using the ferrozine colorimetric method (Stookey 1970),  
185 S<sup>2-</sup> using the methylene blue method (Cline 1969), redox potential with a 220mV offset, pH, and  
186 conductivity using calibrated probes (Orion Ross Ultra pH/ATC Triode, Orion 9179E Triode, Orion  
187 DuraProbe Conductivity Cell), and the remaining sample was acidified to 2% HNO<sub>3</sub> for elemental  
188 analysis using an ICP-OES. The porewater filtered with glass fiber (0.7 $\mu$ m) was acidified with HCl and  
189 analyzed for DOC (Vario TOC Analyzer, Elementar). To characterize the DOC, unacidified DOC





190 samples from the plant maturity sampling event were analyzed via ultraviolet-visible (UV-VIS)/  
191 excitation-emission matrix spectroscopy (EEMs) (Aqualog Spectrophotometer, Horiba). The Aqualog  
192 was zeroed with double deionized water blanks, checked using the manufacturer's excitation check,  
193 corrected for inner filter effects, applied first and second order Rayleigh masking and data were  
194 normalized using the average Raman area (Gao et al. 2011; Clark et al. 2014). Measurements were taken  
195 over the wavelengths of 200-730nm with 2nm steps. Fluorescence and absorbance peaks and indices were  
196 calculated using previously established equations (Table S1).

#### 197 **2.4 Statistical Analysis**

198 Statistical differences between subsites and phenophase were analyzed using repeated measures  
199 analysis of variance (ANOVA) ( $\alpha=0.05$ ), with a post-hoc Tukey-HSD analysis to determine differences  
200 between individual subsites and phenophase. Correlations with depth were analyzed using linear  
201 regression and only the significant ( $p<0.05$ ) relationships are reported. Relationships among all measured  
202 variables were assessed using principal components analysis. In addition, a stepwise regression model  
203 was built to determine variables that significantly predict soil C concentration. All statistical analyses  
204 were conducted in JMP (Version 16.2).

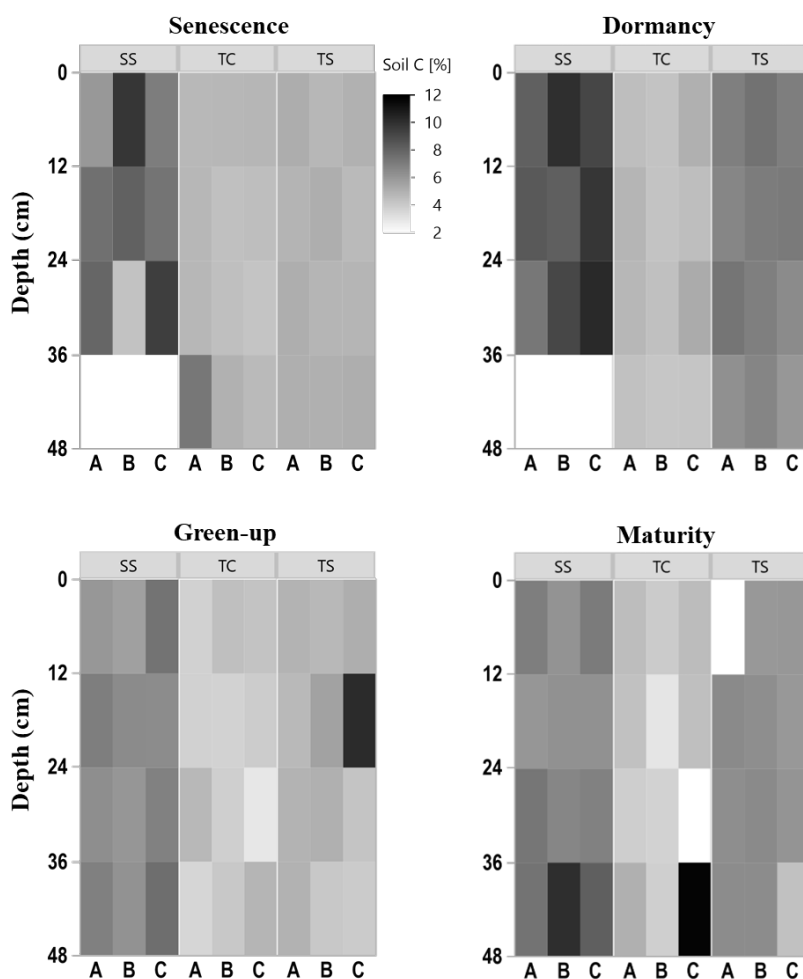
### 205 **3.0 Results**

#### 206 **3.1 Soil Carbon and Sulfur**

207 To explore the spatiotemporal heterogeneity of soil carbon (C) and sulfur (S) at each subsite,  
208 subsamples of each collected soil increment were combusted for soil C and S concentration.  
209 Concentrations of soil C were highly variable among subsites, phenophase, depth, and replicate cores  
210 (Figure 2), indicating several possible sources of variability in marsh soil C stock estimates. SS showed  
211 the highest soil C concentrations, as illustrated by darker colors in the heat map, compared to both TS and  
212 TC. Soil C was also higher at TS than TC, illustrated by relatively darker colors in the heat map. For all  
213 subsites, soil C concentrations changed throughout the year with the highest values during plant  
214 dormancy and the lowest during green-up. However, variability across individual replicates A, B, and C  
215 and with depth complicated generalities across time and space. For example, at subsite SS from 24-36 cm



216 during senescence, core A is ~5% soil C while core C is ~10% soil C, a factor of 2 difference within  
217 replicates. Large ranges among replicates were also observed during green-up at TS from 12-24 cm and  
218 during maturity at TC from 36-48 cm. This exemplifies the heterogeneity inherent in soils, and a source  
219 of variation in marsh soil C estimates.



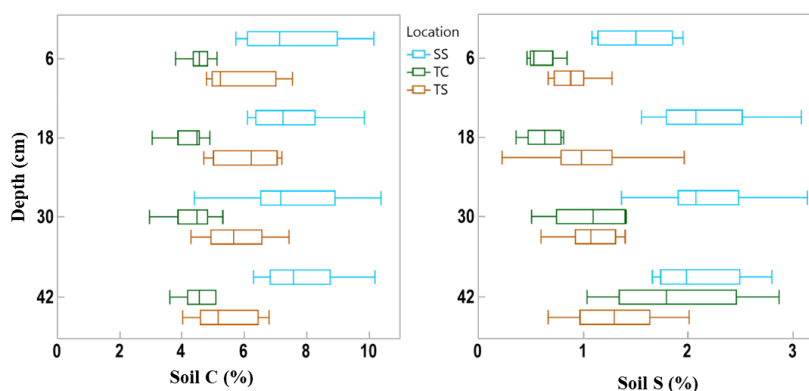
220

221 **Figure 2.** Heat maps of soil C concentration with depth at the three subsites (SS, TC, and TS), four  
222 phenophases, and for each replicate core (A (closest to channel), B, and C (farthest from channel)). No  
223 measurement was able to be obtained for some 12-cm sections as shown by white rectangles.  
224

225 There was also variability in soil C concentration with depth (Figure 3). Subsite SS had the  
226 highest mean soil C concentration at all four depths, as well as the largest range in values. TS had the



227 second highest mean soil C values at all four depths as well as the second largest range in values. TC had  
228 the lowest mean soil C at all four depths as well as the smallest range in values at each depth. It is clear  
229 from this graph that SS contains higher overall concentrations of soil C, followed by TS and then TC. Soil  
230 C at TS during dormancy significantly decreased with depth ( $R^2=0.44$ ,  $p=0.02$ ) and soil C at SS during  
231 maturity significantly increased with depth ( $R^2=0.41$ ,  $p=0.02$ ). No other correlations in soil C existed with  
232 depth.



233

234 **Figure 3.** Box and whisker plot of soil C and S concentrations across the three subsites and separated by  
235 the four sampling depths. This indicates the difference in soil C and S variability among subsites and with  
236 depth. Whiskers indicate the minimum and maximum values, and the box indicates the upper and lower  
237 quartiles. The line in the box indicates the median.

238

239 Soil S also varied across 12 cm sampling increment depths (Figure 3). SS had the highest mean

240 soil S concentration at each depth, and the range of values initially increased with depth. TS has a higher

241 mean concentration than TC at all depths except at the bottom core section. The range of soil S values

242 increased with depth at TC while the range was more consistent with depth at TS, except for the wide

243 range of values measured at the 18cm depth interval. Soil S at SS during maturity significantly increased

244 with depth ( $R^2=0.50$ ,  $p=0.01$ ), as did TC during dormancy ( $R^2=0.88$ ,  $p<0.0001$ ), green-up ( $R^2=0.51$ ,

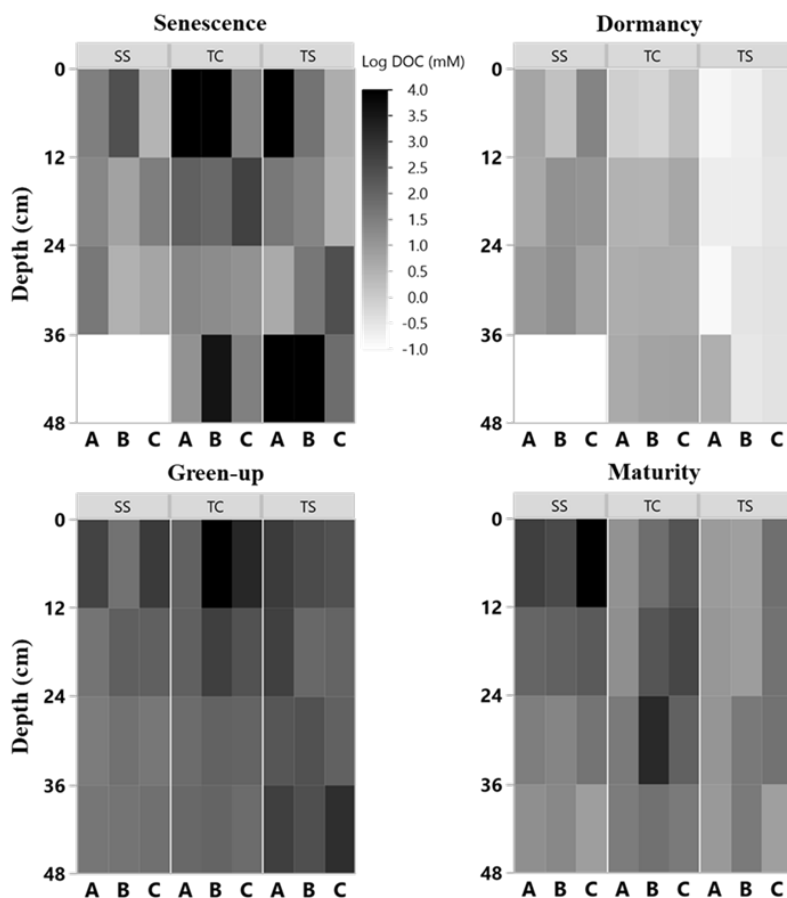
245  $p=0.01$ ), and senescence ( $R^2=0.42$ ,  $p=0.02$ ). No other correlations between soil S existed with depth.

## 246 3.2 Porewater Data

### 247 3.2.1 Porewater DOC and Characterization



248 Porewater DOC was highly variable across subsites, phenophase, depth, and replicate cores  
249 (Figure 4). Note that the data in Figure 4 have been log transformed (natural log) due to large ranges in  
250 values across the one-year sampling campaign. Unlike soil C, which was relatively consistent with depth,  
251 DOC concentrations were highly variable with depth and even more so among replicate cores. Some of  
252 the highest individual concentrations of DOC were detected nearest the surface and rooting zone, which  
253 can extend to 20 cm below the surface (Muench and Elsey-Quirk 2019), but also at depth at SS during  
254 senescence. DOC concentrations decreased with depth at SS during green-up ( $R^2=0.44$ ,  $p=0.02$ ) and  
255 maturity ( $R^2=0.37$ ,  $p=0.03$ ) and increased with depth at TC during dormancy ( $R^2=0.76$ ,  $p=0.0002$ ). These  
256 results indicate the highly variable nature of porewater DOC concentrations, possibly leading to  
257 additional and complexity in marsh soil C estimates.



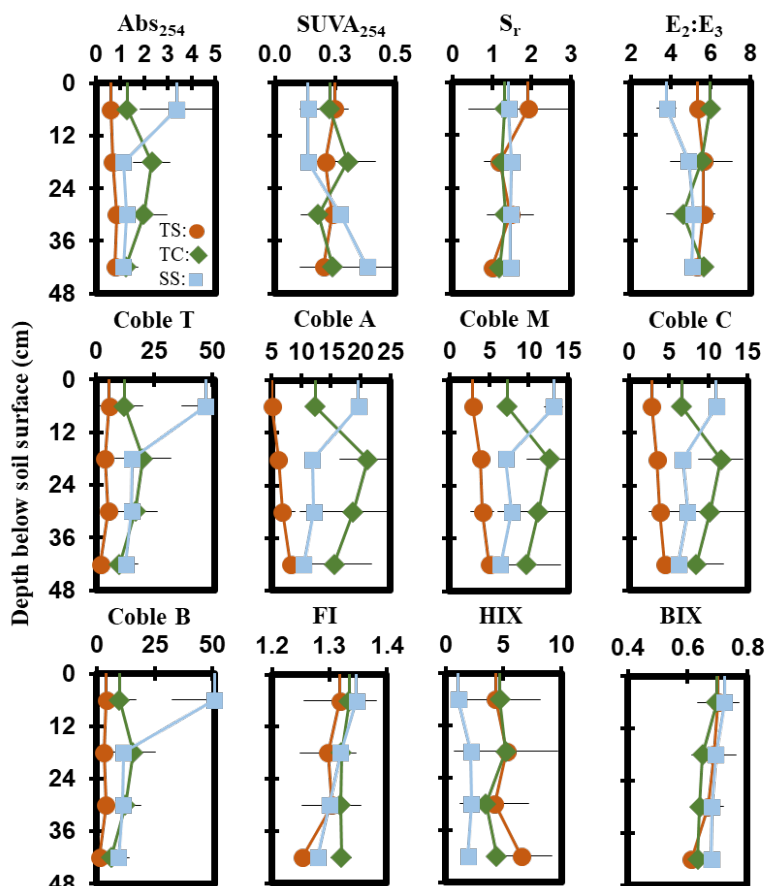
258

259 **Figure 4.** Heat maps of porewater DOC (natural log) concentration with depth at the three subsites (SS,  
 260 TC, and TS), four phenophases, and for each replicate core (A (closest to channel), B, and C (farthest  
 261 from channel)). No measurement was able to be obtained for some 12-cm sections as shown by white  
 262 rectangles.  
 263

264 Porewater ultraviolet-visible (UV-VIS) and excitation emission matrices (EEMs) data were  
 265 collected only from the maturity sampling event to further characterize DOC molecular properties (Figure  
 266 5). Optical properties (i.e., peaks, indices) from spectroscopic data were calculated and interpreted  
 267 following previous studies cited in the supplemental table (Table S1). These data show significant trends  
 268 with depth at SS. At SS, coble peak intensities T ( $R^2=0.55$ ,  $p=0.01$ ), B ( $R^2=0.49$ ,  $p=0.01$ ), A ( $R^2=0.57$ ,  
 269  $p=0.004$ ), M ( $R^2=0.55$ ,  $p=0.01$ ) and C ( $R^2=0.49$ ,  $p=0.01$ ) all significantly decreased with depth, as did the



270 fluorescence index (FI) ( $R^2=0.79$ ,  $p=0.0001$ ), the biological index (BIX) ( $R^2=0.50$ ,  $p<0.01$ ) and  
 271 absorbance at 254nm ( $Abs_{254}$ ) ( $R^2=0.36$ ,  $p=0.04$ ), indicating decreases in CDOM with depth. To ensure  
 272 the coble peaks represented changes in CDOM properties and not DOC concentration, they were  
 273 normalized to DOC concentration and the relationships remained significant ( $p<0.05$ ), except for the  
 274 Coble B peak ( $R^2=0.11$ ,  $p=0.20$ ). The  $E_2:E_3$  ( $R^2=0.50$ ,  $p=0.01$ ) and  $SUVA_{254}$  ( $R^2=0.53$ ,  $p=0.007$ )  
 275 significantly increased with depth at SS, indicating a decrease in molecular weight and an increase in  
 276 aromaticity with depth. No significant trends with depth were present at TC or TS. Differences in DOC  
 277 molecular properties among subsites are apparent for many of the calculated indices and peaks.



278

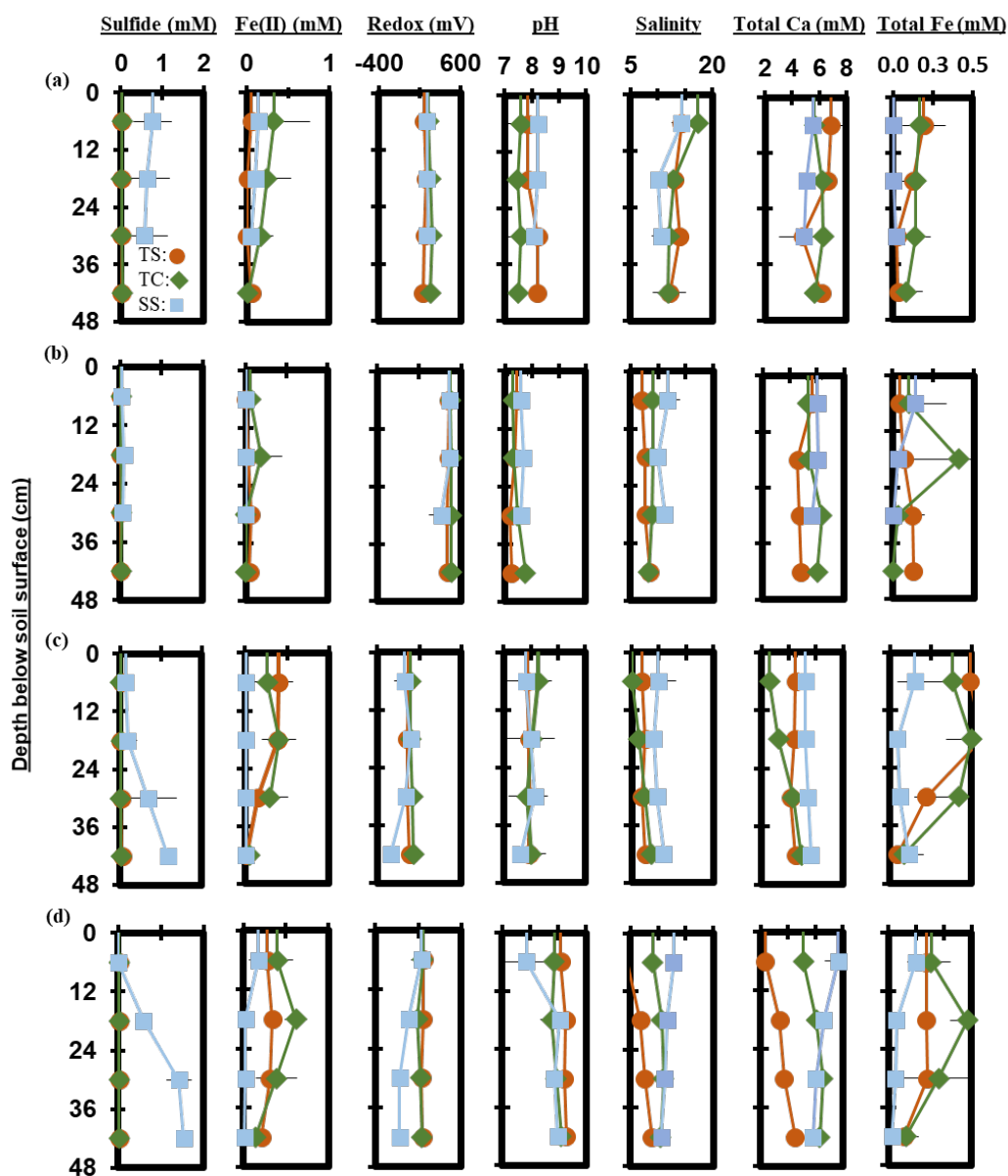
279 **Figure 5.** Depth profiles of porewater EEMs/ UV-VIS peaks and indices down to 48cm taken during the  
 280 maturity sampling event. Each point represents the mean between replicates ( $n=3$ ) with error lines  
 281 indicating the standard deviation ( $\pm 1$  SD).



282

### 283 **3.2.2 Porewater Chemistry**

284 Measured porewater biogeochemistry was variable across subsites, phenophase, and depth  
285 (Figure 6). Porewater redox potentials showed minimal trends with depth, except for a significant  
286 decrease with depth at SS during maturity ( $R^2=0.58$ ,  $p=0.004$ ), though redox showed variability between  
287 replicates (Figure S2). The pH was relatively consistent with depth, except for a significant increase with  
288 depth at TC during dormancy ( $R^2=0.42$ ,  $p=0.02$ ), and a significant decrease with depth at TS during  
289 dormancy ( $R^2=0.56$ ,  $p=0.005$ ). Redox potential and pH formed a significant but weak negative correlation  
290 ( $R^2=0.12$ ,  $p<0.0001$ ) across the entire 1-year dataset.



291

292 **Figure 6.** Depth profiles of porewater chemistry variables down to 48cm for sampling events that  
 293 occurred during plant (a) senescence, (b) dormancy, (c) green-up and (d) maturity. Each point represents  
 294 the mean between replicates (n=3) with error lines indicating the standard deviation ( $\pm 1$  SD).  
 295

296 Porewater  $S^{2-}$  varied significantly with depth.  $S^{2-}$  increased significantly with depth across the  
 297 entire 1-year dataset ( $R^2=0.04$ ,  $p=0.03$ ).  $S^{2-}$  increased significantly with depth at SS during green-up





298 ( $R^2=0.51$ ,  $p=0.01$ ) and maturity ( $R^2=0.86$ ,  $p<0.0001$ ). TS  $S^{2-}$  increased significantly during green-up  
299 ( $R^2=0.46$ ,  $p=0.02$ ) while TC  $S^{2-}$  increased significantly during maturity ( $R^2=0.36$ ,  $p=0.04$ ). Porewater  $Fe^{2+}$   
300 trended negatively with  $S^{2-}$  ( $R^2=0.06$ ,  $p=0.004$ ) and decreased with depth ( $p=0.01$ ,  $R^2=0.05$ ) across the  
301 entire 1-year dataset. Significant decreases were observed at TS during green-up ( $R^2=0.68$ ,  $p=0.001$ ), and  
302 at SS during maturity ( $R^2=0.41$ ,  $p=0.02$ ). Total Fe concentration followed similar depth trends to  $Fe^{2+}$ ,  
303 with a significant decrease with depth across the entire 1-year experiment ( $R^2=0.06$ ,  $p=0.01$ ). Total Fe  
304 decreased with depth at TS during senescence ( $R^2=0.41$ ,  $p=0.03$ ) and green-up ( $R^2=0.58$ ,  $p=0.004$ ), and at  
305 SS during maturity ( $R^2=0.57$ ,  $p=0.01$ ).

306 Porewater salinity formed varying relationships with depth. Salinity significantly decreased with  
307 depth at TC during senescence ( $R^2=0.52$ ,  $p=0.01$ ), and at SS during maturity ( $R^2=0.62$ ,  $p=0.002$ ) while  
308 salinity significantly increased with depth at TC during green-up ( $R^2=0.69$ ,  $p=0.001$ ) and at TS during  
309 maturity ( $R^2=0.87$ ,  $p<0.0001$ ). Salinity and total Ca generally increased together ( $p>0.0001$ ,  $R^2=0.42$ )  
310 across the entire 1-year experiment. Total Ca increased significantly with depth at TC during green-up  
311 ( $R^2=0.86$ ,  $p<0.0001$ ) and at TS ( $R^2=0.80$ ,  $p<0.0001$ ) and TC ( $R^2=0.47$ ,  $p=0.01$ ) during maturity. SS total  
312 Ca significantly decreased with depth during maturity ( $R^2=0.60$ ,  $p=0.005$ ).

### 313 **3.3 Analysis of Variance (ANOVA) Among Subsite and Phenophase**

314 ANOVAs were run on subsite and phenophase mean values that were obtained by averaging  
315 samples from all depths across all four phenophases (for subsite comparisons) and all depths across all  
316 three subsites (for phenophase comparisons). These results show significant spatial and temporal  
317 variability in many of our measured variables. All three subsites contain significantly different average  
318 concentrations of soil C, with SS having the highest average (7.5% C), followed by TS (5.8% C) and TC  
319 (4.6% C). This indicates that on average, subsite SS contains ~29% more soil C than TS and 63% more  
320 soil C than TC. In addition, plant dormancy contained significantly more soil C than plant green-up.  
321 While soil S did not significantly vary across phenophase, soil S at SS was significantly higher in  
322 concentration by a factor of two than both TS and TC.



323 **Table 1.** One-way ANOVA results for all assessed porewater biogeochemical variables. Mean values  
 324 represent average values for each subsite for subsamples from all depths and phenophase. The mean is  
 325 reported ( $\pm$  SD) along with a connecting letter report. Means with letters that do not connect are  
 326 significantly ( $p < 0.05$ ) different.  
 327

Variable	Tall Spartina (TS)	Tall Cordgrass (TC)	Short Spartina (SS)
Soil C (%)	5.8 $\pm$ (1.2) <sup>B</sup>	4.6 $\pm$ (1.3) <sup>C</sup>	7.5 $\pm$ (1.4) <sup>A</sup>
Soil S (%)	1.1 $\pm$ (0.5) <sup>B</sup>	1.0 $\pm$ (0.6) <sup>B</sup>	2.0 $\pm$ (0.7) <sup>A</sup>
DOC (mM)	11.9 $\pm$ (27) <sup>A</sup>	13.6 $\pm$ (27) <sup>A</sup>	7 $\pm$ (9) <sup>A</sup>
Redox (mV)	179 $\pm$ (176) <sup>AB</sup>	211 $\pm$ (185) <sup>A</sup>	93 $\pm$ (235) <sup>B</sup>
pH	8.12 $\pm$ (0.8) <sup>A</sup>	7.99 $\pm$ (0.7) <sup>A</sup>	8.13 $\pm$ (0.6) <sup>A</sup>
Fe <sup>2+</sup> (mM)	0.15 $\pm$ (0.1) <sup>A</sup>	0.22 $\pm$ (0.3) <sup>A</sup>	0.04 $\pm$ (0.1) <sup>B</sup>
Sulfide (mM)	0.02 $\pm$ (0.01) <sup>B</sup>	0.02 $\pm$ (0.01) <sup>B</sup>	0.6 $\pm$ (0.6) <sup>A</sup>
Salinity (ppt)	8.8 $\pm$ (3.1) <sup>B</sup>	9.7 $\pm$ (3) <sup>AB</sup>	11 $\pm$ (2) <sup>A</sup>
Total Fe (mM)	0.21 $\pm$ (0.2) <sup>A</sup>	0.26 $\pm$ (0.3) <sup>A</sup>	0.08 $\pm$ (0.1) <sup>B</sup>
Total Ca (mM)	4.7 $\pm$ (1.3) <sup>B</sup>	5.4 $\pm$ (1.2) <sup>A</sup>	5.8 $\pm$ (0.8) <sup>A</sup>

328

329



330 **Table 2.** One-way ANOVA results for all assessed porewater biogeochemical variables. Mean values  
 331 represent average values for each phenophase for subsamples from all depths and subsites. The mean is  
 332 reported ( $\pm$  SD) along with a connecting letter report. Means with letters that do not connect are  
 333 significantly ( $p < 0.05$ ) different.

Variable	Senescence	Dormancy	Green-up	Maturity
Soil C (%)	5.7 $\pm$ (1.5) <sup>AB</sup>	6.7 $\pm$ (1.1) <sup>A</sup>	5.3 $\pm$ (1.5) <sup>B</sup>	6.1 $\pm$ (1.8) <sup>AB</sup>
Soil S (%)	1.4 $\pm$ (0.7) <sup>A</sup>	1.4 $\pm$ (0.9) <sup>A</sup>	1.4 $\pm$ (0.7) <sup>A</sup>	1.3 $\pm$ (0.7) <sup>A</sup>
DOC (mM)	22.2 $\pm$ (42) <sup>A</sup>	1.6 $\pm$ (1) <sup>B</sup>	12.3 $\pm$ (14) <sup>AB</sup>	7.9 $\pm$ (10) <sup>B</sup>
Redox (mV)	193 $\pm$ (60) <sup>B</sup>	453 $\pm$ (58) <sup>A</sup>	-42 $\pm$ (98) <sup>D</sup>	83 $\pm$ (111) <sup>C</sup>
pH	7.89 $\pm$ (0.4) <sup>B</sup>	7.45 $\pm$ (0.2) <sup>C</sup>	7.96 $\pm$ (0.6) <sup>B</sup>	8.94 $\pm$ (0.5) <sup>A</sup>
Fe <sup>2+</sup> (mM)	0.1 $\pm$ (0.2) <sup>BC</sup>	0.03 $\pm$ (0.1) <sup>C</sup>	0.2 $\pm$ (0.2) <sup>AB</sup>	0.2 $\pm$ (0.2) <sup>A</sup>
Sulfide (mM)	0.2 $\pm$ (0.4) <sup>AB</sup>	0.04 $\pm$ (0.04) <sup>B</sup>	0.2 $\pm$ (0.4) <sup>AB</sup>	0.3 $\pm$ (0.6) <sup>A</sup>
Salinity (ppt)	12.9 $\pm$ (2.4) <sup>A</sup>	9.0 $\pm$ (1.8) <sup>BC</sup>	8.0 $\pm$ (2.1) <sup>C</sup>	9.6 $\pm$ (2.4) <sup>B</sup>
Total Fe (mM)	0.1 $\pm$ (0.1) <sup>B</sup>	0.1 $\pm$ (0.2) <sup>B</sup>	0.3 $\pm$ (0.2) <sup>A</sup>	0.3 $\pm$ (0.2) <sup>A</sup>
Total Ca (mM)	5.8 $\pm$ (1.0) <sup>A</sup>	5.5 $\pm$ (0.7) <sup>A</sup>	4.5 $\pm$ (0.9) <sup>B</sup>	5.3 $\pm$ (1.6) <sup>A</sup>

334

335 DOC concentration also varied among subsites (Table 1) and phenology (Table 2). The average  
 336 DOC concentration at SS was approximately half of that found at TS and TC, but these results are not  
 337 statistically significant due to large variability and ranges in concentration observed across the 1-year  
 338 experiment. This large variability is exemplified by standard deviations that are larger than the means. In  
 339 addition, DOC also varied across phenophases. Dormancy had the lowest mean DOC concentration and  
 340 was significantly lower than senescence by an order of magnitude. Maturity and green-up did not have  
 341 statistically different DOC concentrations. The EEMs/ UV-VIS dataset from plant maturity was analyzed  
 342 based on subsites (Table 3). There were significant differences in peaks and indices between subsites.  
 343 Coble peaks T, A, M, C and Abs<sub>254</sub> were significantly lower at TS than at both TC and SS by at least a  
 344 factor of two which is in line with the lower DOC concentrations observed for TS at maturity (Fig. 4).  
 345 Subsite SS had a significantly lower HIX and E<sub>2</sub>:E<sub>3</sub> than both TS and TC suggesting it to have DOM with



346 less relative humic content and higher average molecule weight. These results indicate significantly  
 347 different DOC molecular characteristics across subsites. EEMs/ UV-VIS data could not be assessed  
 348 across phenology since these data were collected only during plant maturity.

349 **Table 3.** One-way ANOVA results for UV-VIS EEMs during the plant maturity phenophase. Mean  
 350 values represent average values for each subsite for subsamples from all depths. The mean is reported ( $\pm$   
 351 SD) along with a connecting letter report. Means with letters that do not connect are significantly  
 352 ( $p < 0.05$ ) different.

Parameter	Tall Spartina (TS)	Tall Cordgrass (TC)	Short Spartina (SS)
Abs <sub>254</sub>	0.7 $\pm$ (0.2) <sup>B</sup>	1.7 $\pm$ (0.9) <sup>A</sup>	1.7 $\pm$ (1.3) <sup>A</sup>
SUVA <sub>254</sub>	0.2 $\pm$ (0.1) <sup>A</sup>	0.2 $\pm$ (0.1) <sup>A</sup>	0.2 $\pm$ (0.1) <sup>A</sup>
s <sub>r</sub>	1.39 $\pm$ (0.95) <sup>A</sup>	1.27 $\pm$ (0.33) <sup>A</sup>	1.46 $\pm$ (0.28) <sup>A</sup>
E <sub>2</sub> :E <sub>3</sub>	5.5(0.4) <sup>A</sup>	5.4 $\pm$ (1.1) <sup>A</sup>	4.7 $\pm$ (0.7) <sup>B</sup>
Coble T	4.1 $\pm$ (3.8) <sup>B</sup>	14.7 $\pm$ (10.3) <sup>A</sup>	22.6 $\pm$ (16.2) <sup>A</sup>
Coble A	6.6 $\pm$ (2.1) <sup>B</sup>	16.9 $\pm$ (7.02) <sup>A</sup>	13.5 $\pm$ (4.2) <sup>A</sup>
Coble M	4.0 $\pm$ (1.4) <sup>B</sup>	10.2 $\pm$ (4.4) <sup>A</sup>	8.6 $\pm$ (3.1) <sup>A</sup>
Coble C	3.7 $\pm$ (1.2) <sup>B</sup>	9.2 $\pm$ (4.0) <sup>A</sup>	7.8 $\pm$ (2.3) <sup>A</sup>
FI	1.3 $\pm$ (0.6) <sup>A</sup>	1.3 $\pm$ (0.02) <sup>A</sup>	1.3 $\pm$ (0.03) <sup>A</sup>
HIX	5.1 $\pm$ (3.0) <sup>A</sup>	4.4 $\pm$ (3.1) <sup>A</sup>	1.9 $\pm$ (0.6) <sup>B</sup>
BIX	0.7 $\pm$ (0.7) <sup>A</sup>	0.7 $\pm$ (0.03) <sup>A</sup>	0.7 $\pm$ (0.02) <sup>A</sup>

353

354 Differences in porewater chemistry among subsites (Table 1) and phenophase (Table 2) were also  
 355 significant. SS had the lowest average redox potential and was significantly different from TC which had  
 356 the highest, while TS was not significantly different from either SS or TC. Redox potentials were even  
 357 more variable between phenophase where all four phases had significantly different means. The highest  
 358 mean was measured during dormancy and decreased significantly in the order senescence, maturity and  
 359 green-up. The pH was not significantly different across any of the subsites but did change significantly



360 with phenology. Dormancy had the lowest pH which was significantly different from all other  
361 phenophases. Senescence and green-up had a statistically similar mean pH values that were higher than  
362 dormancy, and the porewater pH during maturity was statistically higher than all other phenophases.  
363  $S^{2-}$  also varied significantly among subsites. SS contained on average more than an order of  
364 magnitude greater  $S^{2-}$  than both TS and TC.  $S^{2-}$  is lowest during dormancy but is only significantly  
365 different than maturity which has the highest  $S^{2-}$  mean. Variability in  $Fe^{2+}$  between subsites was opposite  
366 of  $S^{2-}$ . While TS and TC had low concentrations of  $S^{2-}$ , they had high concentrations of  $Fe^{2+}$ , which were  
367 more than double and significantly higher than  $Fe^{2+}$  at SS.  $Fe^{2+}$  concentrations varied with phenology  
368 similar to  $S^{2-}$  where dormancy had the lowest mean which was significantly different only from maturity  
369 when the highest levels of  $Fe^{2+}$  were detected. Differences between subsite total Fe followed the same  
370 trend as  $Fe^{2+}$ , where SS was significantly lower than both TS and TC. Total Fe was lowest during  
371 dormancy and senescence, which were both statistically similar, but different from green-up and maturity.  
372 SS had the highest mean salinity and was significantly different only from TS which had the  
373 lowest mean salinity. Green-up had a significantly lower mean salinity than all other phenophases except  
374 dormancy. Dormancy was only significantly different from senescence, which had the highest mean  
375 salinity. Subsite differences in Ca were similar to salinity where SS had a significantly higher mean Ca  
376 concentration than TS, but not TC. Green-up had the lowest mean Ca concentration which was  
377 significantly different from all other phenophases.

### 378 **3.4 Stepwise Regression Model Results**

379 A stepwise regression model was run across the entire 1-year experiment to determine the most  
380 important biogeochemical predictors of soil C concentration in our dataset (Table 4). The model results  
381 indicate that depth, redox potential, soil S, and sulfide are the best predictors of soil C concentration. The  
382 model  $R^2$  value of 0.44 indicates that these variables explain 44% of the variability in our soil C  
383 concentration data and the model is highly significant ( $p < 0.0001$ ). Sulfide, redox, and soil S each have  
384 positive estimates, meaning that these variables increase as soil C increases while depth had a negative



385 estimate, meaning that soil C tends to decrease with depth across the entire dataset. Each individual  
386 predictor variable is also significant ( $p < 0.05$ ).

387

388 **Table 4.** Stepwise regression results for predicting soil carbon.

Parameter	Estimate	P-Value	Model $R^2$	Model P-Value
Depth	-0.03	0.003	0.44	<0.0001
Sulfide	0.96	0.04		
Redox	0.002	0.002		
Soil S%	1.3	<0.0001		

389

## 390 **4.0 Discussion**

### 391 **4.1 Subsite Differences in Soil C and Biogeochemistry**

392 We hypothesized that soil C concentration and soil biogeochemistry would differ across our  
393 subsite locations. Our results support this hypothesis and suggest significant differences in both soil C  
394 concentration and porewater biogeochemistry among subsites, which is consistent with prior work at this  
395 field site (Seyfferth et al. 2020; Guimond et al. 2020a). This finding illustrates the importance of  
396 considering multiple sampling locations when conducting blue C assessments to account for ecosystem-  
397 scale variability. At SS, average soil C concentrations were 63% higher than at TC and 29% higher than  
398 at TS. Even though these subsites are several to tens of meters from one another, they each had  
399 statistically different mean soil C concentrations. Higher soil C at SS is not related to higher primary  
400 productivity because the *Spartina alterniflora* at SS are stunted. The short form of *S. alterniflora* is  
401 generally less productive than the tall form (Roman and Daiber 1984) and likely exudes less DOC from  
402 the smaller root mass. This is supported by a lower average DOC concentration at SS. Also, the  
403 chromophoric dissolved organic matter (CDOM) properties at SS were different than at the other subsites.  
404 SS CDOM had a significantly lower  $E_2:E_3$  than TS and TC, indicative of higher molecular weight DOC at



405 SS. In addition, the humification index (HIX) was significantly lower at SS indicating that the DOC at SS  
406 has been reworked by microbes less than it has been at TS and TC. Furthermore, SS consistently had  
407 lower porewater redox potentials than the other subsites; while our data represent a snapshot in time for  
408 each phenophase and subsite location, they are consistent with prior work of higher resolution porewater  
409 over time that shows SS being more strongly reducing than areas closer to the tidal channel (Guimond et  
410 al., 2020a; Seyfferth et al. 2020). Redox potentials at SS were low enough to support sulfate reduction.  
411 This is confirmed by our elevated  $S^{2-}$  porewater concentrations measured at SS. Therefore, the greatest  
412 controls on soil C concentration at SS is slower microbial oxidation of C due to strongly reducing  
413 conditions caused by nearly constant inundation and limited flushing of oxygenated surface water  
414 (Guimond et al. 2020b, a; Seyfferth et al. 2020). These conditions lead to CDOM that is less affected by  
415 microbial degradation (i.e., low HIX, low  $E_2:E_3$ ) and a less energetically favorable metabolism (i.e.,  
416 sulfate reduction) resulting in more C storage. This has important implications for soil C stock uncertainty  
417 because a greater amount of the area at St Jones is composed of subsite SS (Seyfferth et al. 2020).  
418 Sampling only near the tidal creek (TS and TC) could significantly underestimate soil C stocks, while  
419 sampling only in the marsh interior could lead to an oversimplification of soil biogeochemistry and DOC  
420 molecular properties in salt marsh ecosystems.

421 In contrast to SS, soil redox potentials were significantly higher at TC and soil C was  
422 significantly lower. This is likely due to TC having a slightly higher elevation on a natural levee and less  
423 reducing surface soils (Seyfferth et al. 2020). The redox potential is not low enough to support sulfate  
424 reduction but is low enough to support Fe reduction. This is supported by the abundant amount of  $Fe^{2+}$   
425 measured in the porewater at TC. A higher redox potential and more energetically favorable electron  
426 acceptor ( $Fe^{3+}$ ) likely leads to higher rates of C mineralization and explains the lower soil C concentration  
427 at TC. On the other hand, we found some of the highest concentrations of DOC at TC, particularly closer  
428 to the surface near the rooting zone. This can be explained by a greater root mass and correspondingly  
429 higher root exudation rate of the taller *S. cynosuroides* coupled with porewater flushing occurring only on  
430 a spring-neap pattern, which allows DOC to build up in porewater over time (Guimond et al. 2020a, b). A



431 higher concentration of freshly produced DOC and a lower concentration of soil C is also consistent with  
432 the priming effect which posits that high concentrations of freshly produced and microbially labile DOC  
433 can stimulate microbial growth leading to the degradation of older, more stable soil C (Textor et al. 2019;  
434 Zhang et al. 2021). In addition, TC CDOM fluorescence peaks (Coble, A, M, C, T), were similar to SS,  
435 indicating that SS and TC have strong sources of fluorescent CDOM.

436         Though TS and TC are biogeochemically more similar than SS, TS had significantly higher soil C  
437 than TC likely due to different dominant vegetation and hydrology. TS is lower in elevation and  
438 experiences diurnal tidal oscillations with slightly lower average porewater redox values than TC (Table  
439 1), which experiences tidal oscillations on a spring-neap cycle (Guimond et al. 2020a). These differences  
440 in hydrology may cause soil C to accumulate more so under slightly stronger reducing conditions at TS  
441 compared to TC. Another unique attribute of subsite TS is the CDOM signature. The coble peaks (A, T,  
442 C, and M) and  $Abs_{254}$  were significantly lower at TS than both TC and SS, which indicates a decreased  
443 concentration of terrestrially-derived CDOM. This is likely because TS is nearest the tidal creek and  
444 therefore porewater solutes are exported to the tidal channel twice daily during ebb tide (Fettrow et al.,  
445 2023b), decreasing the marsh grass derived terrestrial CDOM signature in the near-channel porewater.

#### 446 **4.2 Phenophase Differences in Soil C and Biogeochemistry**

447         We further hypothesized that soil C concentration and biogeochemistry would vary across plant  
448 phenophase, and our data support this hypothesis. Soil C was greatest during plant dormancy and was on  
449 average 26% higher than green-up, 18% higher than senescence, and 10% higher than maturity. This  
450 highlights the importance of considering the time of year soil samples are taken when conducting a blue C  
451 assessment. Likewise, many of the biogeochemical variables also changed with phenophase. The redox  
452 potential of all four phenophases were significantly different from one another, with the highest average  
453 redox potential occurring during dormancy. Higher redox potentials during dormancy are associated with  
454 significantly lower porewater  $Fe^{2+}$  and  $S^{2-}$ , indicating that microbial reduction is likely suppressed during  
455 the winter months when labile DOC produced from root exudation is less available. Dormancy also had  
456 the highest soil C concentration. We suggest this may be related to a suppressed priming affect due to low





457 porewater DOC concentrations and to Fe oxide formation during the high redox potential of dormancy,  
458 allowing any remaining porewater C to be pulled out of solution and into the solid phase with oxidized Fe  
459 minerals (Riedel et al. 2013; Sodano et al. 2017; ThomasArrigo et al. 2019).

460 We found that DOC concentrations are higher during senescence and significantly lower during  
461 plant maturity. High porewater DOC during senescence agrees with previous work showing higher  
462 belowground allocation of biomass in *Spartina* before the winter (Crosby et al. 2015). Belowground  
463 allocation of C in *S. alterniflora* has been shown to increase late into the growing season (Lytle and Hull  
464 1980) while concentrations of soil organics have been shown to decrease during the summer months due  
465 to higher temperatures and higher rates of soil respiration (Caçador et al. 2004). Higher rates of  
466 belowground C allocation during senescence are further supported by the higher rates of soil respiration  
467 during senescence (Vázquez-Lule and Vargas 2021) due to increased labile DOC availability and  
468 associated microbial activity previously reported at this field site.

#### 469 **4.3 Biogeochemical Controls on Soil C**

470 Our data reveal important biogeochemical controls on soil C concentration across space and time.  
471 The results of the stepwise regression model suggest that soil C concentrations are predicted by sulfide,  
472 soil S, redox potential, and depth. Soil C increased significantly with increasing sulfide and soil S  
473 concentration, indicated by the positive model estimate (Table 4). This is likely associated with the lower  
474 elevation, and redox potential and greater accumulation of sulphate at SS due to less tidal flushing. This  
475 may also be a result of sulfurization where inorganic sulfur, namely sulfide, may interact with organic  
476 matter via abiotic reactions (Alperin et al. 1994). Evidence suggests that this interaction can help preserve  
477 and stabilize soil C (Tegelaar et al. 1989), though spectroscopic evidence would be required to determine  
478 if this is an important process at this study site.

479 Depth also has an important control on soil C concentration and the estimate was negative,  
480 indicating that soil C decreases with depth. This is consistent with the literature suggesting higher soil C  
481 concentration at the surface and decreasing with depth in coastal salt marshes (Bai et al. 2016). While  
482 depth was an important predictor of soil C from the stepwise regression model, our depth profiles (Figure



483 4) indicate only small changes with depth. This may be a result of only sampling to 48 cm and integrating  
484 across 12 cm increments, or it may be a result of our method design of extracting porewater from the soils  
485 and running porewater DOC as a separate fraction of C from the solid phase soil C. Because our  
486 porewater DOC results indicate higher concentrations near the surface, the removal of porewater DOC  
487 prior to soil C analysis may lead to lower concentrations of soil C at the surface because in most studies,  
488 porewater DOC is typically incorporated into the bulk soil C measurements upon soil drying and not  
489 extracted as a separate fraction of C (i.e., porewater DOC). We suggest future studies consider porewater  
490 DOC as a separate component of the overall soil C concentration, particularly because the variability with  
491 depth is much higher for porewater DOC than soil C and porewater DOC is presumed to be more labile  
492 and mobile than particulate OC. Therefore, when porewater is extracted from the soil, the measured soil C  
493 concentration may appear less variable with depth and time leading to more consistent estimates of the  
494 more stable solid-phase soil C.

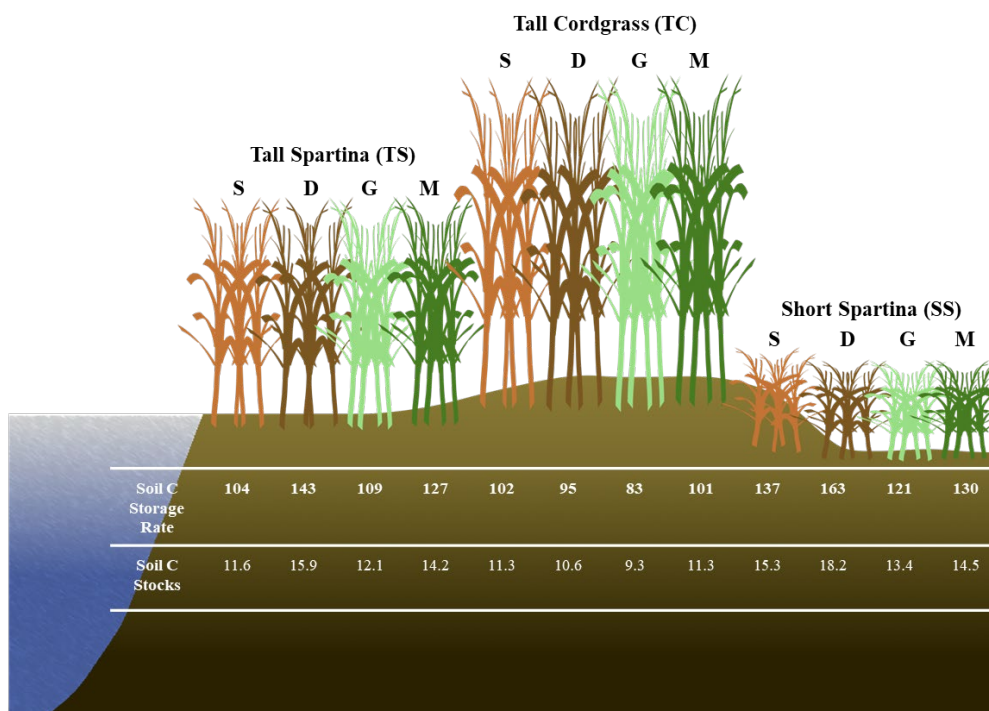
495 Redox potential was the final significant predictor in the stepwise regression model and increased  
496 significantly with soil C. We expected to see a negative relationship between soil C and redox potential  
497 due to higher C preservation under reducing conditions, but an overall positive relationship between  
498 redox potential and soil C in the model indicates an additional and possibly more important mechanism  
499 related to shifting biogeochemistry throughout the year. We observed more oxic conditions at all subsites  
500 during plant dormancy in the winter, probably due to the cold winter conditions that allow for the higher  
501 dissolved oxygen concentrations in water and porewaters observed previously (Trifunovic et al. 2020).  
502 Despite more oxygenated conditions and higher redox potentials in winter, the microbial activity likely  
503 decreased during winter, allowing elevated soil C during the winter months when plants were dormant. In  
504 addition, the less reducing and more oxygenated conditions in winter likely promoted the formation of Fe  
505 oxides that incorporated solution-phase C into the solid phase via coprecipitation. While there is an  
506 abundance of evidence showing the importance of Fe oxides in soil C storage in non-wetland ecosystems  
507 (Lalonde et al. 2012; Riedel et al. 2013; Sowers et al. 2018a, b, 2019; Adhikari et al. 2019), recent studies  
508 have shown the important role of Fe oxides in C cycling in tidal salt marshes (Seyfferth et al. 2020;



509 Fettrow et al. 2023a), but few studies track C cycling during the cool winter months. Variations in Fe  
510 oxide complexation with C due to phenological phase should be further investigated.

#### 511 **4.4 Variability in Soil Carbon Storage Rates and Stocks**

512           Based on soil accretion rates obtained from a previous study near our core locations (Tucker  
513 2016), bulk density at each of the three subsites previously obtained (Wilson and Smith 2015), and our  
514 mean soil C concentrations averaged across depth for each subsite within phenophases, we calculated the  
515 soil C accumulation rates and soil C stocks at each of the three subsites within each of the four  
516 phenophases (Figure 7). These accumulation rates are in range of previously reported values for  
517 mesohaline tidal salt marshes (Chmura et al. 2003; Lovelock et al. 2014; Ye et al. 2015; Mcleod et al.  
518 2016; Macreadie et al. 2017, 2020), as are the soil C stock estimates (Zhao et al. 2016; Ewers Lewis et al.  
519 2018; van Ardenne et al. 2018; Ouyang and Lee 2020; Gorham et al. 2021). These results further illustrate  
520 that soil C storage rates and soil C stocks are highly dynamic and change based on time and space within  
521 a single ecosystem. The largest difference between rates and stocks occurred between SS dormancy and  
522 TC green-up, in which the average storage rates varied by 75% and the average stocks varied by 96%.  
523 Therefore, within the same ecosystem and between phenophases, soil C storage rates and stocks can vary  
524 substantially, leading to variability and uncertainty. To account for spatial and temporal heterogeneity in  
525 soil C storage rates and stocks, we suggest taking soil cores across multiple vegetation zones (if they  
526 exist) and across both the growing and non-growing seasons. This way, more variability can be accounted  
527 for, leading to less uncertainty in blue C estimates.



528

529 **Figure 7.** Conceptual diagram illustrating the spatial and temporal variability of soil C storage rates ( $\text{g C m}^{-2} \text{yr}^{-1}$ ) and soil C stocks ( $\text{kg C m}^{-2}$ ) based on subsites by phenophase. Soil C stocks are to 48cm depth.  
 530 S= senescence, D= dormancy, G= green-up, M= maturity.  
 531  
 532

### 533 5.0 Conclusion

534 Our results highlight the variability in soil C in time and space at the site level. We found that  
 535 some level of uncertainty in estimates of stocks and accumulation rates is likely related to spatial and  
 536 temporal variability of soil C and biogeochemistry at the marsh scale. Subsites that were only a few  
 537 meters from one another contained significantly different soil C concentrations, likely used different  
 538 metabolic pathways for C mineralization, contained significantly different porewater CDOM molecular  
 539 properties and led to considerable variation in soil C storage rates and soil C stock estimates. The  
 540 biogeochemical controls that were best correlated with soil C concentration were redox potential, soil S,  
 541 sulfide, and depth, indicating that the redox potential and sulfur content of the soils are critical in



542 controlling how much soil C accumulates in coastal marsh ecosystems. We also found that soil C  
543 concentration and thus soil C storage rates and soil C stock estimates, varies significantly across the  
544 phenophases of the marsh grasses. Plant dormancy contained the highest mean soil C concentration,  
545 possibly a result of high redox potential during winter months that causes remaining porewater DOC to be  
546 incorporated into the solid phase with oxidized minerals such as Fe oxides and lower microbial activity.  
547 These results demonstrate the importance of considering marsh-scale spatial and temporal heterogeneity  
548 when conducting a blue C assessment. Based on these results, we suggest taking soil cores from multiple  
549 locations within a marsh and in replicate, particularly if multiple types of marsh grass are present, and at  
550 different seasons to account for both spatial and temporal variability. These recommendations may help  
551 lead to less uncertainty in blue C estimates.

552

### 553 **Statements and Declarations**

554 **Competing Interests:** The authors have no relevant financial or non-financial interests to disclose.

555 **Author Contributions:** All authors contributed to the study conception and design. Material preparation,  
556 data collection, and analysis were performed by Sean Fettrow. The first draft of the manuscript was  
557 written by Sean Fettrow and Angelia Seyfferth with edits by Holly Michael and Andrew Wozniak. All  
558 authors commented on previous versions of the manuscript. All authors read and approved the final  
559 manuscript

### 560 **Data Availability Statement**

561 Data is available on Figshare (DOI: 10.6084/m9.figshare.24274417)

### 562 **Acknowledgments**

563 We thank Chloe Kroll for laboratory assistance, the UD Soil Testing Laboratory and the Advanced  
564 Materials Characterization Lab (AMCL) for analytical assistance, and the staff of the Delaware National  
565 Estuarine Research Reserve (DNERR). A.L.S. and H.A.M. acknowledge support from the National  
566 Science Foundation (Grant Nos. 1759879 and 2012484), S.F. acknowledges support from the Delaware  
567 Environmental Institute. The authors acknowledge the land on which they conducted this study is the



568 traditional home of the Lenni-Lenape tribal nation (Delaware nation). The authors report no conflict of  
569 interest.

570

## 571 **References**

- 572 Adhikari, D., Sowers, T., Stuckey, J. W., Wang, X., Sparks, D. L., and Yang, Y.: Formation and redox  
573 reactivity of ferrihydrite-organic carbon-calcium co-precipitates, *Geochim Cosmochim Acta*, 244,  
574 86–98, <https://doi.org/10.1016/j.gca.2018.09.026>, 2019.
- 575 Alperin, M. J., Albert, D. B., and Martens, C. S.: Seasonal variations in production and consumption  
576 rates of dissolved organic carbon in an organic-rich coastal sediment, *Geochim Cosmochim Acta*,  
577 58, 4909–4930, [https://doi.org/10.1016/0016-7037\(94\)90221-6](https://doi.org/10.1016/0016-7037(94)90221-6), 1994.
- 578 van Ardenne, L. B., Jolicouer, S., Bérubé, D., Burdick, D., and Chmura, G. L.: The importance of  
579 geomorphic context for estimating the carbon stock of salt marshes, *Geoderma*, 330, 264–275,  
580 <https://doi.org/10.1016/j.geoderma.2018.06.003>, 2018.
- 581 Arias-Ortiz, A., Masqué, P., Garcia-Orellana, J., Serrano, O., Mazarrasa, I., Marbà, N., Lovelock, C. E.,  
582 Lavery, P. S., and Duarte, C. M.: Reviews and syntheses: 210Pb-derived sediment and carbon  
583 accumulation rates in vegetated coastal ecosystems –setting the record straight, *Biogeosciences*,  
584 15, 6791–6818, <https://doi.org/10.5194/bg-15-6791-2018>, 2018.
- 585 Bai, J., Zhang, G., Zhao, Q., Lu, Q., Jia, J., Cui, B., and Liu, X.: Depth-distribution patterns and control  
586 of soil organic carbon in coastal salt marshes with different plant covers, *Sci Rep*, 6,  
587 <https://doi.org/10.1038/srep34835>, 2016.
- 588 Baustian, M. M., Stagg, C. L., Perry, C. L., Moss, L. C., Carruthers, T. J. B., and Allison, M.:  
589 Relationships Between Salinity and Short-Term Soil Carbon Accumulation Rates from Marsh Types  
590 Across a Landscape in the Mississippi River Delta, *Wetlands*, 37, 313–324,  
591 <https://doi.org/10.1007/s13157-016-0871-3>, 2017.
- 592 Blair, N. E. and Aller, R. C.: The fate of terrestrial organic carbon in the Marine environment, *Ann*  
593 *Rev Mar Sci*, 4, 401–423, <https://doi.org/10.1146/annurev-marine-120709-142717>, 2012.
- 594 Breithaupt, J. L., Smoak, J. M., Bianchi, T. S., Vaughn, D. R., Sanders, C. J., Radabaugh, K. R., Osland,  
595 M. J., Feher, L. C., Lynch, J. C., Cahoon, D. R., Anderson, G. H., Whelan, K. R. T., Rosenheim, B. E.,  
596 Moyer, R. P., and Chambers, L. G.: Increasing Rates of Carbon Burial in Southwest Florida Coastal  
597 Wetlands, *J Geophys Res Biogeosci*, 125, 1–25, <https://doi.org/10.1029/2019JG005349>, 2020.
- 598 van de Broek, M., Temmerman, S., Merckx, R., and Govers, G.: Controls on soil organic carbon  
599 stocks in tidal marshes along an estuarine salinity gradient, *Biogeosciences*, 13, 6611–6624,  
600 <https://doi.org/10.5194/bg-13-6611-2016>, 2016.
- 601 Van De Broek, M., Temmerman, S., Merckx, R., and Govers, G.: Controls on soil organic carbon  
602 stocks in tidal marshes along an estuarine salinity gradient, *Biogeosciences*, 13, 6611–6624,  
603 <https://doi.org/10.5194/bg-13-6611-2016>, 2016.



- 604 Caçador, I., Costa, A. L., and Vale, C.: Carbon storage in tagus salt marsh sediments, *Water, Air, and*  
605 *Soil Pollution: Focus*, 4, 701–714, <https://doi.org/10.1023/B:WAFO.0000028388.84544.ce>, 2004.
- 606 Capocci, M., Barba, J., Seyfferth, A. L., and Vargas, R.: Experimental influence of storm-surge  
607 salinity on soil greenhouse gas emissions from a tidal salt marsh, *Science of the Total Environment*,  
608 686, 1164–1172, <https://doi.org/10.1016/j.scitotenv.2019.06.032>, 2019.
- 609 Chen, C. and Sparks, D. L.: Multi-elemental scanning transmission X-ray microscopy-near edge X-  
610 ray absorption fine structure spectroscopy assessment of organo-mineral associations in soils from  
611 reduced environments, *Environmental Chemistry*, 12, 64–73, <https://doi.org/10.1071/EN14042>,  
612 2015.
- 613 Chen, C., Dynes, J. J., Wang, J., and Sparks, D. L.: Properties of Fe-organic matter associations via  
614 coprecipitation versus adsorption, *Environ Sci Technol*, 48, 13751–13759,  
615 <https://doi.org/10.1021/es503669u>, 2014.
- 616 Chmura, G. L., Anisfeld, S. C., Cahoon, D. R., and Lynch, J. C.: Global carbon sequestration in tidal,  
617 saline wetland soils, *Global Biogeochem Cycles*, 17, 1111, <https://doi.org/10.1029/2002GB001917>,  
618 2003.
- 619 Clark, C. D., Aiona, P., Keller, J. K., and de Bruyn, W. J.: Optical characterization and distribution of  
620 chromophoric dissolved organic matter (CDOM) in soil porewater from a salt marsh ecosystem,  
621 *Mar Ecol Prog Ser*, 516, 71–83, <https://doi.org/10.3354/meps10833>, 2014.
- 622 Cline, J. D.: SPECTROPHOTOMETRIC DETERMINATION OF HYDROGEN SULFIDE IN NATURAL  
623 WATERS<sup>1</sup>, *Limnol Oceanogr*, 14, 454–458, <https://doi.org/10.4319/lo.1969.14.3.0454>, 1969.
- 624 Crosby, S. C., Ivens-Duran, M., Bertness, M. D., Davey, E., Deegan, L. A., and Leslie, H. M.: Flowering  
625 and biomass allocation in U.S. Atlantic coast *Spartina alterniflora*, *Am J Bot*, 102, 669–676,  
626 <https://doi.org/10.3732/ajb.1400534>, 2015.
- 627 Cuellar-Martinez, T., Ruiz-Fernández, A. C., Sanchez-Cabeza, J. A., Pérez-Bernal, L., López-Mendoza,  
628 P. G., Carnero-Bravo, V., Agraz-Hernández, C. M., van Tussenbroek, B. I., Sandoval-Gil, J., Cardoso-  
629 Mohedano, J. G., Vázquez-Molina, Y., and Aldana-Gutiérrez, G.: Temporal records of organic  
630 carbon stocks and burial rates in Mexican blue carbon coastal ecosystems throughout the  
631 Anthropocene, *Glob Planet Change*, 192, 103215,  
632 <https://doi.org/10.1016/j.gloplacha.2020.103215>, 2020.
- 633 Cusack, M., Saderne, V., Arias-Ortiz, A., Masqué, P., Krishnakumar, P. K., Rabaoui, L., Qurban, M. A.,  
634 Qasem, A. M., Prihartato, P., Loughland, R. A., Elyas, A. A., and Duarte, C. M.: Organic carbon  
635 sequestration and storage in vegetated coastal habitats along the western coast of the Arabian  
636 Gulf, *Environmental Research Letters*, 13, 074007, <https://doi.org/10.1088/1748-9326/aac899>,  
637 2018.
- 638 Davy, A. J., Brown, M. J. H., Mossman, H. L., and Grant, A.: Colonization of a newly developing salt  
639 marsh: disentangling independent effects of elevation and redox potential on halophytes, *Journal*  
640 *of Ecology*, 99, 1350–1357, <https://doi.org/10.1111/j.1365-2745.2011.01870.x>, 2011.



- 641 Desai, A. R.: Climatic and phenological controls on coherent regional interannual variability of  
642 carbon dioxide flux in a heterogeneous landscape, *J Geophys Res*, 115, G00J02,  
643 <https://doi.org/10.1029/2010JG001423>, 2010.
- 644 Dorau, K., Pohl, L., Just, C., Höschen, C., Ufer, K., Mansfeldt, T., and Mueller, C. W.: Soil Organic  
645 Matter and Phosphate Sorption on Natural and Synthetic Fe Oxides under in Situ Conditions,  
646 *Environ Sci Technol*, 53, 13081–13087, <https://doi.org/10.1021/acs.est.9b03260>, 2019.
- 647 Duarte, C. M.: Reviews and syntheses: Hidden forests, the role of vegetated coastal habitats in the  
648 ocean carbon budget, *Biogeosciences*, 14, 301–310, <https://doi.org/10.5194/bg-14-301-2017>,  
649 2017.
- 650 Ewers Lewis, C. J., Carnell, P. E., Sanderman, J., Baldock, J. A., and Macreadie, P. I.: Variability and  
651 Vulnerability of Coastal ‘Blue Carbon’ Stocks: A Case Study from Southeast Australia, *Ecosystems*,  
652 21, 263–279, <https://doi.org/10.1007/s10021-017-0150-z>, 2018.
- 653 Ewers Lewis, C. J., Baldock, J. A., Hawke, B., Gadd, P. S., Zawadzki, A., Heijnis, H., Jacobsen, G. E.,  
654 Rogers, K., and Macreadie, P. I.: Impacts of land reclamation on tidal marsh ‘blue carbon’ stocks,  
655 *Science of the Total Environment*, 672, 427–437, <https://doi.org/10.1016/j.scitotenv.2019.03.345>,  
656 2019.
- 657 Fettrow, S., Vargas, R., and Seyfferth, A. L.: Experimentally simulated sea level rise destabilizes  
658 carbon-mineral associations in temperate tidal marsh soil, *Biogeochemistry*, 163, 103–120,  
659 <https://doi.org/10.1007/s10533-023-01024-z>, 2023a.
- 660 Fettrow, S., Jeppi, V., Wozniak, A., Vargas, R., Michael, H., and Seyfferth, A. L.: Physiochemical  
661 Controls on the Horizontal Exchange of Blue Carbon Across the Salt Marsh-Tidal Channel Interface,  
662 *J Geophys Res Biogeosci*, <https://doi.org/10.1029/2023JG007404>, 2023b.
- 663 Ford, H., Garbutt, A., Duggan-Edwards, M., Pagès, J. F., Harvey, R., Ladd, C., and Skov, M. W.: Large-  
664 scale predictions of salt-marsh carbon stock based on simple observations of plant community and  
665 soil type, *Biogeosciences*, 16, 425–436, <https://doi.org/10.5194/bg-16-425-2019>, 2019.
- 666 Frasco, B. A. and Good, R. E.: Decomposition Dynamics of *Spartina alterniflora* and *Spartina patens*  
667 in a New Jersey Salt Marsh, *Am J Bot*, 69, 402, <https://doi.org/10.2307/2443145>, 1982.
- 668 Gao, L., Fan, D., Sun, C., Li, D., and Cai, J.: Optical characterization of CDOM in a marsh-influenced  
669 environment in the Changjiang (Yangtze River) Estuary, *Environ Earth Sci*, 64, 643–658,  
670 <https://doi.org/10.1007/s12665-010-0885-8>, 2011.
- 671 Gorham, C., Lavery, P., Kelleway, J. J., Salinas, C., and Serrano, O.: Soil Carbon Stocks Vary Across  
672 Geomorphic Settings in Australian Temperate Tidal Marsh Ecosystems, *Ecosystems*, 24, 319–334,  
673 <https://doi.org/10.1007/s10021-020-00520-9>, 2021.
- 674 Guimond, J. A., Seyfferth, A. L., Moffett, K. B., and Michael, H. A.: A physical-biogeochemical  
675 mechanism for negative feedback between marsh crabs and carbon storage, *Environmental*  
676 *Research Letters*, 15, 034024, <https://doi.org/10.1088/1748-9326/ab60e2>, 2020a.





- 677 Guimond, J. A., Yu, X., Seyfferth, A. L., and Michael, H. A.: Using Hydrological-Biogeochemical  
678 Linkages to Elucidate Carbon Dynamics in Coastal Marshes Subject to Relative Sea Level Rise,  
679 *Water Resour Res*, 56, 1–16, <https://doi.org/10.1029/2019WR026302>, 2020b.
- 680 Kang, X., Hao, Y., Cui, X., Chen, H., Huang, S., Du, Y., Li, W., Kardol, P., Xiao, X., and Cui, L.:  
681 Variability and Changes in Climate, Phenology, and Gross Primary Production of an Alpine Wetland  
682 Ecosystem, *Remote Sens (Basel)*, 8, 391, <https://doi.org/10.3390/rs8050391>, 2016.
- 683 Koretsky, C. M., Van Cappellen, P., Dichristina, T. J., Kostka, J. E., Lowe, K. L., Moore, C. M.,  
684 Roychoudhury, A. N., and Viollier, E.: Salt marsh pore water geochemistry does not correlate with  
685 microbial community structure, *Estuar Coast Shelf Sci*, 62, 233–251,  
686 <https://doi.org/10.1016/j.ecss.2004.09.001>, 2005.
- 687 Lacroix, E. M., Mendillo, J., Gomes, A., Dekas, A., and Fendorf, S.: Contributions of anoxic microsites  
688 to soil carbon protection across soil textures, *Geoderma*, 425,  
689 <https://doi.org/10.1016/j.geoderma.2022.116050>, 2022.
- 690 Lalonde, K., Mucci, A., Ouellet, A., and G elinas, Y.: Preservation of organic matter in sediments  
691 promoted by iron, *Nature*, 483, 198–200, <https://doi.org/10.1038/nature10855>, 2012.
- 692 Lovelock, C. E., Adame, M. F., Bennion, V., Hayes, M., O’Mara, J., Reef, R., and Santini, N. S.:  
693 Contemporary rates of carbon sequestration through vertical accretion of sediments in mangrove  
694 forests and saltmarshes of South East Queensland, Australia, *Estuaries and Coasts*,  
695 <https://doi.org/10.1007/s12237-013-9702-4>, 2014.
- 696 Luo, M., Liu, Y., Huang, J., Xiao, L., Zhu, W., Duan, X., and Tong, C.: Rhizosphere processes induce  
697 changes in dissimilatory iron reduction in a tidal marsh soil: a rhizobox study, *Plant Soil*, 433, 83–  
698 100, <https://doi.org/10.1007/s11104-018-3827-y>, 2018.
- 699 Luo, M., Huang, J.-F., Zhu, W.-F., and Tong, C.: Impacts of increasing salinity and inundation on  
700 rates and pathways of organic carbon mineralization in tidal wetlands: a review, *Hydrobiologia*,  
701 827, 31–49, <https://doi.org/10.1007/s10750-017-3416-8>, 2019.
- 702 Lytle, R. W. and Hull, R. J.: Annual Carbohydrate Variation in Culms and Rhizomes of Smooth  
703 Cordgrass (*Spartina alterniflora* Loisel.) 1 , *Agron J*, 72, 942–946,  
704 <https://doi.org/10.2134/agronj1980.00021962007200060019x>, 1980.
- 705 Macreadie, P. I., Ollivier, Q. R., Kelleway, J. J., Serrano, O., Carnell, P. E., Ewers Lewis, C. J., Atwood,  
706 T. B., Sanderman, J., Baldock, J., Connolly, R. M., Duarte, C. M., Lavery, P. S., Steven, A., and  
707 Lovelock, C. E.: Carbon sequestration by Australian tidal marshes, *Sci Rep*, 7, 44071,  
708 <https://doi.org/10.1038/srep44071>, 2017.
- 709 Macreadie, P. I., Anton, A., Raven, J. A., Beaumont, N., Connolly, R. M., Friess, D. A., Kelleway, J. J.,  
710 Kennedy, H., Kuwae, T., Lavery, P. S., Lovelock, C. E., Smale, D. A., Apostolaki, E. T., Atwood, T. B.,  
711 Baldock, J., Bianchi, T. S., Chmura, G. L., Eyre, B. D., Fourqurean, J. W., Hall-Spencer, J. M., Huxham,  
712 M., Hendriks, I. E., Krause-Jensen, D., Laffoley, D., Luisetti, T., Marb a, N., Masque, P., McGlathery,  
713 K. J., Megoigal, J. P., Murdiyarsa, D., Russell, B. D., Santos, R., Serrano, O., Silliman, B. R.,  
714 Watanabe, K., and Duarte, C. M.: The future of Blue Carbon science, *Nat Commun*, 10, 3998,  
715 <https://doi.org/10.1038/s41467-019-11693-w>, 2019.



- 716 Macreadie, P. I., Nielsen, D. A., Kelleway, J. J., Atwood, T. B., Seymour, J. R., Petrou, K., Connolly, R.  
717 M., Thomson, A. C. G., Stacey, M., and Ralph, P. J.: Can we manage coastal ecosystems to  
718 sequester more blue carbon?, *15*, 206–213, 2020.
- 719 Mcleod, E., Chmura, G. L., Bouillon, S., Salm, R., Björk, M., Duarte, C. M., Lovelock, C. E.,  
720 Schlesinger, W. H., and Silliman, B. R.: A blueprint for blue carbon: toward an improved  
721 understanding of the role of vegetated coastal habitats in sequestering CO<sub>2</sub>, *Front Ecol Environ*, *9*,  
722 552–560, <https://doi.org/https://www.jstor.org/stable/41479959>, 2016.
- 723 Mcowen, C., Weatherdon, L., Bochove, J.-W., Sullivan, E., Blyth, S., Zockler, C., Stanwell-Smith, D.,  
724 Kingston, N., Martin, C., Spalding, M., and Fletcher, S.: A global map of saltmarshes, *Biodivers Data*  
725 *J*, *5*, e11764, <https://doi.org/10.3897/BDJ.5.e11764>, 2017.
- 726 McTigue, N., Davis, J., Rodriguez, A. B., McKee, B., Atencio, A., and Currin, C.: Sea Level Rise  
727 Explains Changing Carbon Accumulation Rates in a Salt Marsh Over the Past Two Millennia, *J*  
728 *Geophys Res Biogeosci*, *124*, 2945–2957, <https://doi.org/10.1029/2019JG005207>, 2019.
- 729 Miller, C. B., Rodriguez, A. B., Bost, M. C., McKee, B. A., and McTigue, N. D.: Carbon accumulation  
730 rates are highest at young and expanding salt marsh edges, *Commun Earth Environ*, *3*,  
731 <https://doi.org/10.1038/s43247-022-00501-x>, 2022.
- 732 Moffett, K. and Gorlick, S.: Relating salt marsh pore water geochemistry patterns to vegetation  
733 zones and hydrologic influences, *J Am Water Resour Assoc*, *52*, 1729–1745,  
734 <https://doi.org/10.1111/j.1752-1688.1969.tb04897.x>, 2016.
- 735 Mueller, P., Ladiges, N., Jack, A., Schmiedl, G., Kutzbach, L., Jensen, K., and Nolte, S.: Assessing the  
736 long-term carbon-sequestration potential of the semi-natural salt marshes in the European  
737 Wadden Sea, *Ecosphere*, *10*, <https://doi.org/10.1002/ecs2.2556>, 2019.
- 738 Muench, A. and Elsey-Quirk, T.: Competitive reversal between plant species is driven by species-  
739 specific tolerance to flooding stress and nutrient acquisition during early marsh succession, *Journal*  
740 *of Applied Ecology*, *56*, 2236–2247, <https://doi.org/10.1111/1365-2664.13458>, 2019.
- 741 Negandhi, K., Edwards, G., Kelleway, J. J., Howard, D., Safari, D., and Saintilan, N.: Blue carbon  
742 potential of coastal wetland restoration varies with inundation and rainfall, *Sci Rep*, *9*, 4368,  
743 <https://doi.org/10.1038/s41598-019-40763-8>, 2019.
- 744 Negrin, V. L., Spetter, C. V., Asteasuain, R. O., Perillo, G. M. E., and Marcovecchio, J. E.: Influence of  
745 flooding and vegetation on carbon, nitrogen, and phosphorus dynamics in the pore water of a  
746 *Spartina alterniflora* salt marsh, *Journal of Environmental Sciences*, *23*, 212–221,  
747 [https://doi.org/10.1016/S1001-0742\(10\)60395-6](https://doi.org/10.1016/S1001-0742(10)60395-6), 2011.
- 748 Ouyang, X. and Lee, S. Y.: Improved estimates on global carbon stock and carbon pools in tidal  
749 wetlands, <https://doi.org/10.1038/s41467-019-14120-2>, 2020.
- 750 Riedel, T., Zak, D., Biester, H., and Dittmar, T.: Iron traps terrestrially derived dissolved organic  
751 matter at redox interfaces, *Proceedings of the National Academy of Sciences*, *110*, 10101–10105,  
752 <https://doi.org/10.1073/pnas.1221487110>, 2013.



- 753 Roman, C. T. and Daiber, F. C.: Aboveground and Belowground Primary Production Dynamics of  
754 Two Delaware Bay Tidal Marshes, *Torrey Botanical Society*, 111, 34–41,  
755 <https://doi.org/https://www.jstor.org/stable/2996208>, 1984.
- 756 Saintilan, N., Rogers, K., Mazumder, D., and Woodroffe, C.: Allochthonous and autochthonous  
757 contributions to carbon accumulation and carbon store in southeastern Australian coastal  
758 wetlands, *Estuar Coast Shelf Sci*, 128, 84–92, <https://doi.org/10.1016/j.ecss.2013.05.010>, 2013.
- 759 Sanders, C. J., Maher, D. T., Tait, D. R., Williams, D., Holloway, C., Sippo, J. Z., and Santos, I. R.: Are  
760 global mangrove carbon stocks driven by rainfall?, *J Geophys Res Biogeosci*, 121, 2600–2609,  
761 <https://doi.org/10.1002/2016JG003510>, 2016.
- 762 Serrano, O., Lovelock, C. E., B. Atwood, T., Macreadie, P. I., Canto, R., Phinn, S., Arias-Ortiz, A., Bai,  
763 L., Baldock, J., Bedulli, C., Carnell, P., Connolly, R. M., Donaldson, P., Esteban, A., Ewers Lewis, C. J.,  
764 Eyre, B. D., Hayes, M. A., Horwitz, P., Hutley, L. B., Kavazos, C. R. J., Kelleway, J. J., Kendrick, G. A.,  
765 Kilminster, K., Lafratta, A., Lee, S., Lavery, P. S., Maher, D. T., Marbà, N., Masque, P., Mateo, M. A.,  
766 Mount, R., Ralph, P. J., Roelfsema, C., Rozaimi, M., Ruhon, R., Salinas, C., Samper-Villarreal, J.,  
767 Sanderman, J., J. Sanders, C., Santos, I., Sharples, C., Steven, A. D. L., Cannard, T., Trevathan-  
768 Tackett, S. M., and Duarte, C. M.: Australian vegetated coastal ecosystems as global hotspots for  
769 climate change mitigation, *Nat Commun*, 10, 4313, <https://doi.org/10.1038/s41467-019-12176-8>,  
770 2019.
- 771 Seyfferth, A. L., Bothfeld, F., Vargas, R., Stuckey, J. W., Wang, J., Kearns, K., Michael, H. A.,  
772 Guimond, J., Yu, X., and Sparks, D. L.: Spatial and temporal heterogeneity of geochemical controls  
773 on carbon cycling in a tidal salt marsh, *Geochim Cosmochim Acta*, 282, 1–18,  
774 <https://doi.org/10.1016/j.gca.2020.05.013>, 2020.
- 775 Smeaton, C., Barlow, N. L. M., and Austin, W. E. N.: Coring and compaction: Best practice in blue  
776 carbon stock and burial estimations, *Geoderma*, 364, 114180,  
777 <https://doi.org/10.1016/j.geoderma.2020.114180>, 2020.
- 778 Sodano, M., Lerda, C., Nisticò, R., Martin, M., Magnacca, G., Celi, L., and Said-Pullicino, D.:  
779 Dissolved organic carbon retention by coprecipitation during the oxidation of ferrous iron,  
780 *Geoderma*, 307, 19–29, <https://doi.org/10.1016/j.geoderma.2017.07.022>, 2017.
- 781 Sowers, T. D., Adhikari, D., Wang, J., Yang, Y., and Sparks, D. L.: Spatial Associations and Chemical  
782 Composition of Organic Carbon Sequestered in Fe, Ca, and Organic Carbon Ternary Systems,  
783 *Environ Sci Technol*, 52, 6936–6944, <https://doi.org/10.1021/acs.est.8b01158>, 2018a.
- 784 Sowers, T. D., Stuckey, J. W., and Sparks, D. L.: The synergistic effect of calcium on organic carbon  
785 sequestration to ferrihydrite, *Geochem Trans*, 19, 22–26, <https://doi.org/10.1186/s12932-018-0049-4>, 2018b.
- 787 Sowers, T. D., Holden, K. L., Coward, E. K., and Sparks, D. L.: Dissolved Organic Matter Sorption and  
788 Molecular Fractionation by Naturally Occurring Bacteriogenic Iron (Oxyhydr)oxides, *Environ Sci  
789 Technol*, 53, 4295–4304, <https://doi.org/10.1021/acs.est.9b00540>, 2019.
- 790 Stookey, L. L.: Ferrozine-A New Spectrophotometric Reagent for Iron, *Anal Chem*, 42, 779–781,  
791 <https://doi.org/10.1021/ac60289a016>, 1970.



- 792 Tegelaar, E. W., de Leeuw, J. W., Derenne, S., and Largeau, C.: A reappraisal of kerogen formation,  
793 *Geochim Cosmochim Acta*, 53, 3103–3106, [https://doi.org/10.1016/0016-7037\(89\)90191-9](https://doi.org/10.1016/0016-7037(89)90191-9), 1989.
- 794 Textor, S. R., Wickland, K. P., Podgorski, D. C., Johnston, S. E., and Spencer, R. G. M.: Dissolved  
795 Organic Carbon Turnover in Permafrost-Influenced Watersheds of Interior Alaska: Molecular  
796 Insights and the Priming Effect, *Front Earth Sci (Lausanne)*, 7,  
797 <https://doi.org/10.3389/feart.2019.00275>, 2019.
- 798 ThomasArrigo, L. K., Kaegi, R., and Kretzschmar, R.: Ferrihydrite Growth and Transformation in the  
799 Presence of Ferrous Iron and Model Organic Ligands, *Environ Sci Technol*, 53, 13636–13647,  
800 <https://doi.org/10.1021/acs.est.9b03952>, 2019.
- 801 Trifunovic, B., Vázquez-Lule, A., Capooci, M., Seyfferth, A. L., Moffat, C., and Vargas, R.: Carbon  
802 Dioxide and Methane Emissions From A Temperate Salt Marsh Tidal Creek, *J Geophys Res*  
803 *Biogeosci*, 125, <https://doi.org/10.1029/2019JG005558>, 2020.
- 804 Tucker, K. J.: VARIABILITY OF ORGANIC CARBON ACCUMULATION ON A TIDAL WETLAND COAST,  
805 University of Delaware, 2016.
- 806 Valle, J., Gonsior, M., Harir, M., Enrich-Prast, A., Schmitt-Kopplin, P., Bastviken, D., Conrad, R., and  
807 Hertkorn, N.: Extensive processing of sediment pore water dissolved organic matter during anoxic  
808 incubation as observed by high-field mass spectrometry (FTICR-MS), *Water Res*, 129,  
809 <https://doi.org/10.1016/j.watres.2017.11.015>, 2018.
- 810 Vázquez-Lule, A. and Vargas, R.: Biophysical drivers of net ecosystem and methane exchange  
811 across phenological phases in a tidal salt marsh, *Agric For Meteorol*, 300, 108309,  
812 <https://doi.org/10.1016/j.agrformet.2020.108309>, 2021.
- 813 Wang, F., Sanders, C. J., Santos, I. R., Tang, J., Schuerch, M., Kirwan, M. L., Kopp, R. E., Zhu, K., Li, X.,  
814 Yuan, J., Liu, W., and Li, Z.: Global blue carbon accumulation in tidal wetlands increases with  
815 climate change, *Natl Sci Rev*, 8, <https://doi.org/10.1093/nsr/nwaa296>, 2021.
- 816 Whitby, H., Planquette, H., Cassar, N., Bucciarelli, E., Osburn, C. L., Janssen, D. J., Cullen, J. T.,  
817 González, A. G., Völker, C., and Sarthou, G.: A call for refining the role of humic-like substances in  
818 the oceanic iron cycle, *Sci Rep*, 10, 6144, <https://doi.org/10.1038/s41598-020-62266-7>, 2020.
- 819 Wilson, K. and Smith, E.: Marsh Carbon Storage in the National Estuarine Research Reserves, USA,  
820 67, 2015.
- 821 Windham, L.: Comparison of biomass production and decomposition between *Phragmites australis*  
822 (common reed) and *spartina patens* (salt hay grass) in brackish tidal marshes of New Jersey, USA,  
823 *Wetlands*, 21, 179–188, [https://doi.org/10.1672/0277-5212\(2001\)021\[0179:COBPAD\]2.0.CO;2](https://doi.org/10.1672/0277-5212(2001)021[0179:COBPAD]2.0.CO;2),  
824 2001.
- 825 Wordofa, D. N., Adhikari, D., Dunham-Cheatham, S. M., Zhao, Q., Poulson, S. R., Tang, Y., and Yang,  
826 Y.: Biogeochemical fate of ferrihydrite-model organic compound complexes during anaerobic  
827 microbial reduction, *Science of the Total Environment*, 668, 216–223,  
828 <https://doi.org/10.1016/j.scitotenv.2019.02.441>, 2019.



- 829 Ye, S., Laws, E. A., Yuknis, N., Ding, X., Yuan, H., Zhao, G., Wang, J., Yu, X., Pei, S., and DeLaune, R.  
830 D.: Carbon Sequestration and Soil Accretion in Coastal Wetland Communities of the Yellow River  
831 Delta and Liaohe Delta, China, *Estuaries and Coasts*, <https://doi.org/10.1007/s12237-014-9927-x>,  
832 2015.
- 833 Yousefi Lalimi, F., Silvestri, S., D'Alpaos, A., Roner, M., and Marani, M.: The Spatial Variability of  
834 Organic Matter and Decomposition Processes at the Marsh Scale, *J Geophys Res Biogeosci*, 123,  
835 3713–3727, <https://doi.org/10.1029/2017JG004211>, 2018.
- 836 Yu, J., Dong, H., Li, Y., Wu, H., Guan, B., Gao, Y., Zhou, D., and Wang, Y.: Spatiotemporal Distribution  
837 Characteristics of Soil Organic Carbon in Newborn Coastal Wetlands of the Yellow River Delta  
838 Estuary, *Clean (Weinh)*, 42, 311–318, <https://doi.org/10.1002/clen.201100511>, 2014.
- 839 Zhang, D., Gong, C., Zhang, W., Zhang, H., Zhang, J., and Song, C.: Labile carbon addition alters soil  
840 organic carbon mineralization but not its temperature sensitivity in a freshwater marsh of  
841 Northeast China, *Applied Soil Ecology*, 160, <https://doi.org/10.1016/j.apsoil.2020.103844>, 2021.
- 842 Zhao, Q., Bai, J., Liu, Q., Lu, Q., Gao, Z., and Wang, J.: Spatial and Seasonal Variations of Soil Carbon  
843 and Nitrogen Content and Stock in a Tidal Salt Marsh with *Tamarix chinensis*, China, *Wetlands*, 36,  
844 145–152, <https://doi.org/10.1007/s13157-015-0647-1>, 2016.
- 845 Zhu, Q., Cochran, J. K., Heilbrun, C., Yin, H., Feng, H., Tamborski, J. J., Fitzgerald, P., and Cong, W.:  
846 Small-Scale Geochemical Heterogeneities and Seasonal Variation of Iron and Sulfide in Salt  
847 Marshes Revealed by Two-Dimensional Sensors, *Front Earth Sci (Lausanne)*, 9,  
848 <https://doi.org/10.3389/feart.2021.653698>, 2021.
- 849